BRNO UNIVERSITY OF TECHNOLOGY

Faculty of Chemistry

MASTER'S THESIS

Brno, 2019 Bc. Matej Dzurov

BRNO UNIVERSITY OF TECHNOLOGY
VYSOKÉ UČENÍ TECHNICKÉ V BRNĚ

FACULTY OF CHEMISTRY
FAKULTA CHEMICKÁ

INSTITUTE OF MATERIALS SCIENCE
ÚSTAV CHEMIE MATERIÁLŮ

THE EFFECT OF POLYMER MICROFIBERS ON RHEOLOGICAL AND MECHANICAL PROPERTIES OF CALCIUM PHOSPHATE BONE CEMENTS

VLIV POLYMERNÍCH MIKROVLÁKEN NA REOLOGICKÉ A MECHANICKÉ VLASTNOSTI KOSTNÍCH CEMENTŮ Z FOSFOREČNANU VÁPENATÉHO

MASTER'S THESIS
DIPLOMOVÁ PRÁCE

AUTHOR — **Bc. Matej Dzurov**
AUTOR PRÁCE

SUPERVISOR — **doc. Ing. Lucy Vojtová, Ph.D.**
VEDOUCÍ PRÁCE

BRNO 2019

BRNO FACULTY UNIVERSITY OF CHEMISTRY OF TECHNOLOGY

Master's Thesis Assignment

Number of thesis:	FCH-DIP1334/2018	Academic year: 2018/19
Institute:	Institute of Materials Science	
Student:	**Bc. Matej Dzurov**	
Study programme:	Chemistry, Technology and Properties of Materials	
Study field:	Chemistry, Technology and Properties of Materials	
Head of thesis:	**doc. Ing. Lucy Vojtová, Ph.D.**	

Title of Master's Thesis:

The effect of polymer microfibers on rheological and mechanical properties of calcium phosphate bone cements

Master's Thesis assignment:

1) literary research on micro and nanofibers of phosphate cements
2) preparing samples of cements with different contents of polymeric microfibers
3) rheological and mechanical sample testing
4) evaluation
5) conclusion

Deadline for Master's Thesis delivery: 10. 5. 2019

Master's Thesis is necessary to deliver to a secretary of institute in the number of copies defined by the dean. This assignment is part of Master's Thesis.

Bc. Matej Dzurov	doc. Ing. Lucy Vojtová, Ph.D.	doc. Ing. František Šoukal, Ph.D.
Student	Head of thesis	Head of institute

In Brno, 31. 1. 2019

prof. Ing. Martin Weiter, Ph.D.
Dean

ABSTRACT

Proposed master's thesis focuses on mechanical and rheological properties of biodegradable polymer-calcium phosphate bone cement composite reinforced with PCL (poly(ε-caprolactone)) and PCL-Pluronic polymer microfibers.

The theoretical part describes bone structure, evolution of bone cements and structural additives. In the experimental part, synthesis and characterization of PLGA-PEG-PLGA thermosensitive copolymer and α-tricalcium phosphate powder is depicted as well as microfibers preparation technique. Copolymer aqueous solution was used to counteract the paste limited injectability, where liquid to powder (L/P) ratio of 0.5 ml/g was used for all of the samples. The two different mixing techniques were used in cement preparation to modulate the sample's porosity. PCL and PCL-Pluronic fibers used to reinforce the cement were added in the amount of 1, 3 and 5 wt. % to the total mass of cement paste. Prepared pastes were studied at the laboratory (23 °C) and under physiological conditions (37 °C) using dynamical rheological analysis, with the aim to establish workability and setting of the paste. Samples for the rest of the analyses were enabled to set at physiological conditions for the duration of 10 days. Afterward, mechanical parameters like compressive strength, elastic modulus and diametric tensile strength of dried and in some cases hydrated samples were tested. Porosity was established using micro-computed tomography. Scanning electron microscopy was used to study microstructure and fiber incorporation into a ceramic matrix. Presence of fibers was semi-quantitatively studied using Fourier transformed infrared spectroscopy. X-ray diffraction provided data about powder phase transformation and mineralogical aspects of cement. Individual sample performances were evaluated and compared.

As a result, addition of either hydrophobic PCL or amphiphilic PCL-Pluronic fibers into polymer-phosphate cement slightly increased compressive strength where PCL-Pluronic modified fibers performed better. Therefore was concluded, that polymer-phosphate bone cement reinforced with microfibers is promising candidate for surgical practice.

KEYWORDS

calcium phosphate bone cement, α-TCP, PLGA-PEG-PLGA thermosensitive copolymer, biodegradability, fiber reinforcement, mechanical properties, rheology,

ABSTRAKT

Táto diplomová práca sa zaoberá mechanickými a reologickými vlastnosťami resorbovateľného polymér-fosforečnanového kompozitu na báze kostného cementu vystuženého mikrovláknami z PCL (poly(ε-kaprolaktón)) a Pluronic-om modifikovanými PCL vláknami.

Teoretická časť popisuje štruktúru kostí, vývoj kostných cementov a štrukturálne prídavky (aditíva). V experimentálnej časti je rozoberaná syntéza a charakterizácia PLGA-PEG-PLGA termosenzitívneho kopolyméru a α- modifikácie fosforečnanu vápenatého ako aj technika prípravy mikrovláken. Roztok kopolyméru bol použitý pre zlepšenie obmedzenej injektovateľnosti pasty s pomerom kvapalnej k práškovej fáze (L/P) 0,5 ml/g pre všetky vzorky. Dve rôzne techniky zamiešania pasty boli použité pre možnosť kontrolovania porozity pripraveného cementu. PCL a PCL-Pluronic vlákna využité ako výstuž boli testované v troch rôznych prídavkoch, a to 1, 3 a 5 hmotnostných percent vláken na celkovú hmotnosť pripravenej pasty. Pripravené pasty boli testované pomocou dynamickej reologickéj analýzy na reometri pri laboratórnej teplote (23 °C) a fyzologických podmienkach (37 °C) so zámerom stanoviť spracovateľnosť a tuhnutie pasty. Vzorkám na ostatok analýz bolo umožnené vytvrdzovanie pri fyziologických podmienkach po dobu 10 dní. Po vytvrdení boli testované mechanické parametre ako sú pevnosť v tlaku, Youngov modul pružnosti a pevnosť v ťahu v priemere vysušených a v niektorých prípadoch aj hydratovaných vzoriek. Porozita vzoriek bola stanovená pomocou Roentgénovej počítačovej mikro-tomografie. Rastrovacia elektrónová mikroskopia bola využitá na študovanie mikroštruktúry a zabudovanie vláken do keramickej matrice. Prítomnosť vláken bola semi-kvantitatívne stanovená pomocou Fourier transformovanej infračervenej spektroskopie. Difrakcia Roentgénového žiarenia poskytla údaje o fázovom prechode prášku a jeho mineralogickom zložení. Jednotlivé hodnoty, obdržané z jednotlivých analýz, boli medzi sebou porovnané a adekvátne diskutované.

Výsledkom práce je potvrdenie mierneho zlepšenia pevnosti v tlaku vzoriek vystužených hydrofóbnymi PCL alebo amfifilnými PCL-Pluronic vláknami pričom, PCL-Pluronic vlákna poskytli lepšie výsledky. Preto bolo usúdené, že polymér-fosforečnanový kostný cement vystužený vláknami je nádejným kandidátom na uplatnenie v chirurgickej praxi.

KĽÚČOVÉ SLOVÁ

kostné cementy na báze fosforečnanu vápenatého, α-TCP, PLGA-PEG-PLGA termosenzitívny kopolymér, biodegradovateľnosť, výstuž vláknami, mechanické vlastnosti, reológia

DZUROV, M. *Vliv polymerních mikrovláken na reologické a mechanické vlastnosti kostních cementů z fosforečnanu vápenatého.* Brno: Vysoké učení technické v Brně, Fakulta chemická, 2019. 64 s. Vedoucí diplomové práce doc. Ing. Lucy Vojtová, Ph.D.

DZUROV, Matej. *The effect of polymer microfibers on rheological and mechanical properties of calcium phosphate bone cements*. Brno, 2019. Master's thesis. Brno University of Technology, Faculty of Chemistry. 64 p. Supervisor: doc. Ing. Lucy Vojtová, Ph.D.

DECLARATION

I declare that the master's thesis has been worked out by myself and that all the quotations from the used literary sources are accurate and complete. The content of the diploma thesis is the property of the Faculty of Chemistry of Brno University of Technology and Central European Institute of Technology (CEITEC). All commercial uses are allowed only if approved by both the supervisor and the dean of the Faculty of Chemistry, BUT.

.....

Student's signature

ACKNOWLEDGEMENT

I would like to extend my utmost gratitude to all the people that were involved in solving of this master's thesis. My special thanks goes especially to doc. Ing. Lucy Vojtová, Ph.D. for her professional guidance and trust, which enabled me to work on this perspective project with applications in the bioimplantology sector.

A next thanks go to consultants for their contribution to the thesis: M. Sc. Edgar Benjamin Montufar Jimenez, Ph.D., and Ing. Karel Slámečka, Ph.D. with powder synthesis, help and valuable consults during mechanical tests, Ing. Kristýna Valová with help in rheological measurements, Ing. Jana Dorazilová with FTIR analysis, Ing. Marek Zbončák, Ph.D. with help in SEM imaging, Mgr. Jan Žídek, Ph.D. with the interpretation of micro-CT measurements and Bc. Klára Lysáková in copolymer synthesis. For provided measurements and fiber synthesis InoCURE l.t.d., doc. Ing. Klára Částková, Ph.D., and Ing. Jana Brtníková, Ph.D. deserve my thanks as well.

Last but not least, I'd like to thank my parents for material and moral support during all of my studies, and my brother Jakub for English grammar checks.

TABLE OF CONTENTS

1. INTRODUCTION

Calcium phosphate bone cements have been well known for at least 30 years as a candidate for bone regeneration applications. Their advantageous inorganic structure, strikingly resembling bone minerals like hydroxyapatite, in vivo self-setting ability at physiological conditions and the possibility of injectability make them a point of interest in the development of novel resorbable bone cements. Possibility of use in the minimally invasive surgery applications and treatment of bone-related complications e.g. fractures, osteoporosis, and many others, make this material even more perspective candidate for bioimplantology.

Although some properties are advantageous and promising, others are not. Since calcium phosphate cements are hydraulic bioceramics, their brittleness, and inferior mechanical parameters compared to native bone, mainly low flexibility due to lack of collagen, are the major factor, which has to be improved to ensure the best material's performance. The rapid setting of the bone cements i.e. transformation of the main constituent tricalcium phosphate to calcium-deficient hydroxyapatite causes problems with paste's injectability at low levels of force. High solid content without the occurrence of separation demonstrates washout resistance to body fluids soon after mixing, which is again undesirable. Although the cement is made from bone minerals, its low porosity hinders cell growth on the material's surface. This slows down the bone regeneration even though building blocks for bone repair are present.

To counteract these negative properties, the use of biodegradable polymeric additives including polymer fibers increasing injectability behavior, reducing the brittleness and increasing mechanical properties, is proposed as an alternative approach for bone cement modification. Additives not only increase mentioned rheological and mechanical properties, but their biodegradability works in favor of pore formation which increases osteoconductivity of material, resulting in speeding up the healing process.

This thesis, therefore, observes mentioned mechanical and rheological properties of polymer additives and fiber-modified bone cements, evaluating their performance and discussing the effects of added constituents to develop composite material possessing desired properties, which can be "tailor-made" for bone regeneration applications.

2. THEORETICAL PART

2.1. Bone

Skeleton and its constituents – bones, are supporting and protective part of vertebrate organisms. Important functions of bones are namely production of red and white blood cells in bone marrow, storage of minerals like calcium and phosphorus, structural support and a possibility of mobility accompanied by the function of muscles. At birth, the human body is comprised of over 270 bones but during development, some bones fuse together leaving the adult human body with 206 bones [1][2].

2.1.1. Bone structure

Bones are made of bone cells and bone matrix. There are four distinct species of bone cells. Osteoprogenitor cells are undifferentiated stem cells capable of turning into other bone cells like osteoblasts, osteoclasts, and osteocytes. Osteoblasts are responsible for the synthesis of organic components of the matrix and play a role in the deposition of inorganic minerals. Osteoclasts function in bone resorption and in breaking down of the bone tissue to repair or otherwise change bones. Lastly, osteocytes are the most common bone cells, regulating and controlling the activity of osteoclasts and osteoblasts. The function of these cells is dynamic; highly stressed parts of bones are remodeled or reinforced to handle more stress and vice versa.

The bone matrix contains high inorganic content exceeding 50 % of bone's weight. Inorganic constituents are comprised mainly of calcium phosphates arranged into hydroxyapatite crystals in shapes of slabs or plates. Mineral phases of bone are responsible for toughness and strength of bone. Organic content of the matrix is predominantly made up of collagen, which is responsible for bone's elasticity. Bone matrix is therefore highly durable and tough yet flexible to a certain extent, making it optimal supporting material for living organisms.

Tissue within the bone is woven in two main patterns, fibrous and lamellar. The fibrous bone tissue is characterized by entangled collagen fibrils in the intercellular matter, lamellar tissue shows a parallel arrangement of collagen fibrils, forming lamellas. These lamellar structures form either cortical (compact) bones or cancellous (spongy) bones, each with quite different characteristics [2].

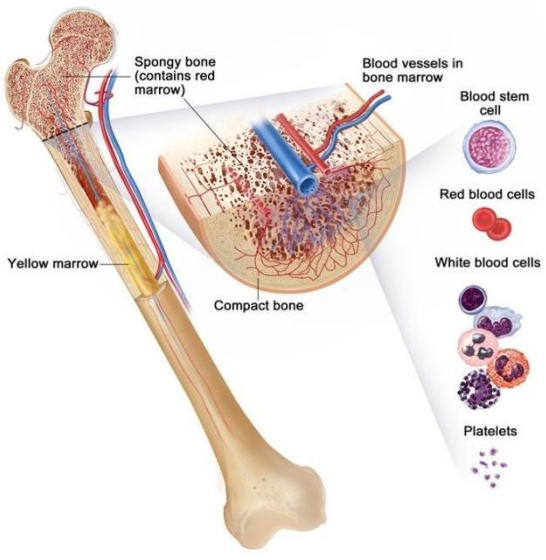

Figure 1: Femur diagram depicting compact bone, spongy bone and bone marrow [3].

Cortical bone, found in an outer layer of bones forms hard bone exterior. The primary anatomical unit cell of cortical bone is osteon, which is a microscopic column made up from lamelles. The entire outer layer is covered by dense collagen ligament called periosteum, inside layer is covered by similar endosteum. Cancellous bone also called trabecular bone is a less dense internal tissue of skeletal bone with a high surface area which forms an open cell porous network. High surface area and porosity enable metabolic activities like calcium exchange to take place and present pores contain a large number of blood vessels, often containing red bone marrow which is responsible for production of red and white blood cells as well as platelets [4]. Even though cortical bone is much denser than cancellous bone, it still possesses some porosity represented by a network of canals and blood vessels of Haversian systems [5].

To sum up, bones are highly complex as well as vital bodily structures and any complications either external, structural or pathological may cause serious harm to the body and its functions.

2.1.2. Complications

Fractures are the most common bone complications; average person suffers from two bone fractures during their lifetime [6]. It is a medical condition in which there is a partial or complete breakage due to an overload of mechanical stress on the continuous bone. In severe cases, the bone may break or get crushed into several pieces leading to comminuted fracture which causes serious healing complications. Other fracture complications include various infections and so-called compartment syndrome; a blockage of blood flow to the local area leading to oxygen deprivation and consecutive necrosis of affected tissues. Even though bones possess high toughness, durability, and strength due to certain medical conditions such as osteoporosis or bone cancer, minimal trauma injuries are possible and commonly referred to as pathologic fractures [7].

Osteoporosis, from Greek, literally meaning “porous bones”, is a disease characterized by a decrease of bone density. It is a major public health problem, affecting hundreds of millions of people worldwide, predominantly elderly, especially postmenopausal women due to the insufficiency of the hormone estrogen. The most commonly affected bones include vertebrae, elbow, forearm, pelvis, hip, femur, and humerus [8]. Prevention of the early development of osteoporosis includes lifestyle changes, proper diet, regular exercise, and fall prevention [9].

Infection of bone or osteomyelitis is classified by duration (acute or chronic), pathogenesis (trauma, contiguous spread, hematogenous, surgical), site, extent, or type of patient. Main causes of the condition are bacteria and to lesser extent fungi, depending on pathogenesis namely *Staphylococcus aureus*, *Streptococcus agalactiae*, *Escherichia coli* or *Mycobacterium tuberculosis* are recovered from affected tissue and blood. These pathogens cluster around bone or bone defect (fracture) which is filled with hematoma and fibrous tissue, creating a perfect breeding ground for the spread of the disease which is often complicated to treat, treatment usually involves large doses of antimicrobial drugs and often surgery [10].

Surgical procedures are sometimes inevitable to solve cartilage or structural bone problems. One of the most commonly performed procedures is total hip arthroplasty, which the hip joint is repaired, remodeled or even completely removed and replaced by endoprosthesis. Despite the fact that the procedure is quite common and with high success rate, surgery is still invasive, and quite difficult. It requires removal of the femoral head from the acetabulum, cutting the ball off using a power saw, and drilling a hole of adequate shape into the femur to insert endoprosthetic metal shaft. During the procedure, small bone fragments and bacteria may be unintentionally introduced to damaged bone, leading to complications like osteomyelitis [11].

2.2. Bone cements

Speeding up the recovery from various fractures, reduction or total eradication of infectious growths in post-surgery patients, and better fixation of endoprosthetics are just a few applications where properly modified, biocompatible, and possibly resorbable bone cements propose a new and arguably better solution to bone damage.

2.2.1. PMMA cement

In today's arthroplasty practice acrylic polymer called polymethyl methacrylate (PMMA) bone cement is widely used to secure the endoprosthetic implant in the bone. Cement fixation relies on the formation of a strong mechanical bond between cement and bone. PMMA bone cement is applied to the smooth surface of the endoprosthesis in two to three-centimeter layer to ensure a proper bond between bone and metal stem. Afterward, the endoprosthesis is secured in the bone.

Although cement itself is sufficient enough for these applications, this solution is more recommended to less active patients, patients over age 60 and patients with poor bone quality, density or suffering from certain conditions like rheumatoid arthritis. Due to the application of excessive amounts of stress to cement, the prosthesis may get loose or cement may wear down leaving fragments which in turn cause inflammatory reaction [11]. Even though PMMA is biocompatible, unfortunately, it's not bioresorbable or bioactive and stays in body forever. Some sources even claim that polymerization is said to kill osteocytes due to elevated temperature during setting reaction [12] and monomer methyl methacrylate (MMA) is considered to be irritant or even carcinogen [13].

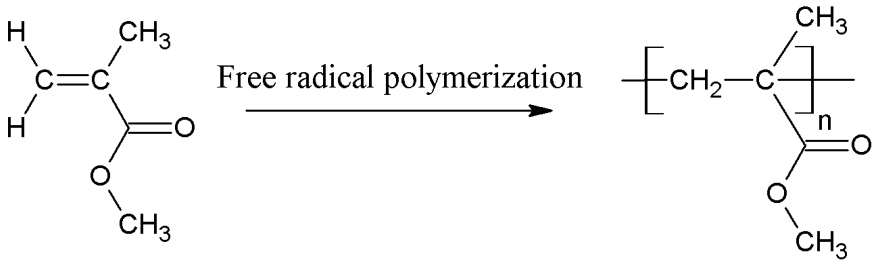

Figure 2: Reaction schematic of methyl methacrylate polymerization to PMMA [56].

2.2.2. Calcium phosphate cement

Thanks to their advantageous biocompatibility, bioactivity, osteoconductivity, and possible injectability, calcium phosphate cements (CPCs) are considered as an alternative replacement for PMMA polymer cements. Injectability of CPCs presents a solution to surgeries by introducing so-called minimum invasive surgery, where CPC paste is deposited to damaged bone via syringe. CPCs also possess intrinsic microporosity due to the formation of intergranular spaces while undergoing setting reaction [14].

Currently, CPCs are defined as a combination of one or more calcium phosphate powders which, upon mixing with a liquid phase, form a paste, able to self-set and harden *in situ* at the bone defect site [14]. The main mechanisms of self-setting reaction include dissolution and reprecipitation. During dissolution calcium and phosphate ions are liberated from powder, saturating solution until the solution reaches critical threshold supersaturation. Consecutively reprecipitation begins, forming nuclei of a new phase. The growth of new phase continues with the dissolution of reagents until their depletion. Determination of emergence of a new phase is represented by a function of pH, dependent on the logarithmic concentration of calcium or phosphate ions in solution. According to the saturated solutions pH value at 37 °C, apatite phases for pH > 4.2, or brushite, known also as dicalcium phosphate dihydrate

(DCPD) for pH < 4.2, may form [15]. Desirable apatite phases, namely hydroxyapatite (HA) and analogous calcium deficient hydroxyapatite (CDHA) formed during said conditions are main building blocks of bones which make them the perfect candidates for bone reparation. Introduction of water to CPCs results in the formation of CDHA according to equation 1 forming desired bone mineral [16].

$$3\,Ca_3(PO_4)_2 + H_2O \rightarrow\ Ca_9(HPO_4)(PO_4)_5(OH) \qquad (1)$$

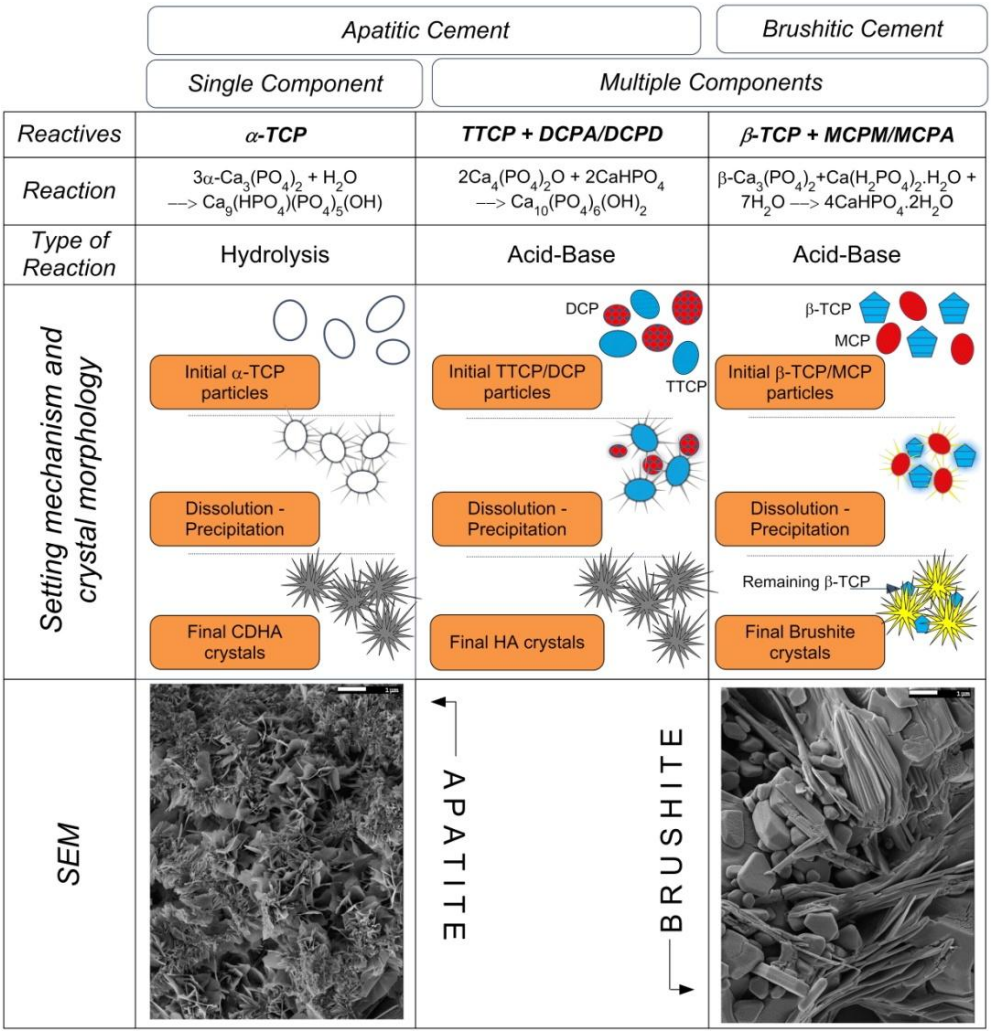

Figure 3: Overview of main structural and morphological differences between apatitic and brushitic calcium phosphate cements[55].

2.3. Calcium phosphates

Calcium phosphates (CPs) are the largest group of artificial bone replacements due to their close resemblance to the mineral components of bone. Fine tuning the final cement composition, geometrical properties of individual components, and resorption characteristics of produced material leads to bone cement, possessing desired porosity and high mechanical strength [17]. Most notable calcium phosphates are namely monoclinic α- and rhombohedral β- phases of tricalcium phosphates (TCPs).

Although α- and β- phase both have the same chemical composition, structural variabilities are present which affect density and solubility, in turn affecting the field of application. β-TCP is used mainly for preparing biodegradable bioceramics shaped as dense and macro-porous granules and blocks, whereas the more soluble and reactive α-TCP is used mainly as a

fine powder in the preparation of calcium phosphate cements. α- and β-TCP are currently used in several clinical applications in dentistry, maxillo-facial surgery and orthopedics: β-TCP is the component of several commercial mono- or biphasic bioceramics and composites, and α-TCP is the major constituent of the powder component of various hydraulic bone cements [18].

2.3.1. Structural characteristics

TCPs can be classified by their temperature stability into two groups, low-temperature modification of β-TCP and high-temperature modifications represented by α-TCP and α'-TCP. The α'- phase lacks practical interest due to stability only at temperatures above 1430 °C, cooling of α'-TCP results phase transition into metastable α-TCP. Composition and temperature relation is depicted in the phase diagram in Figure 4 [18].

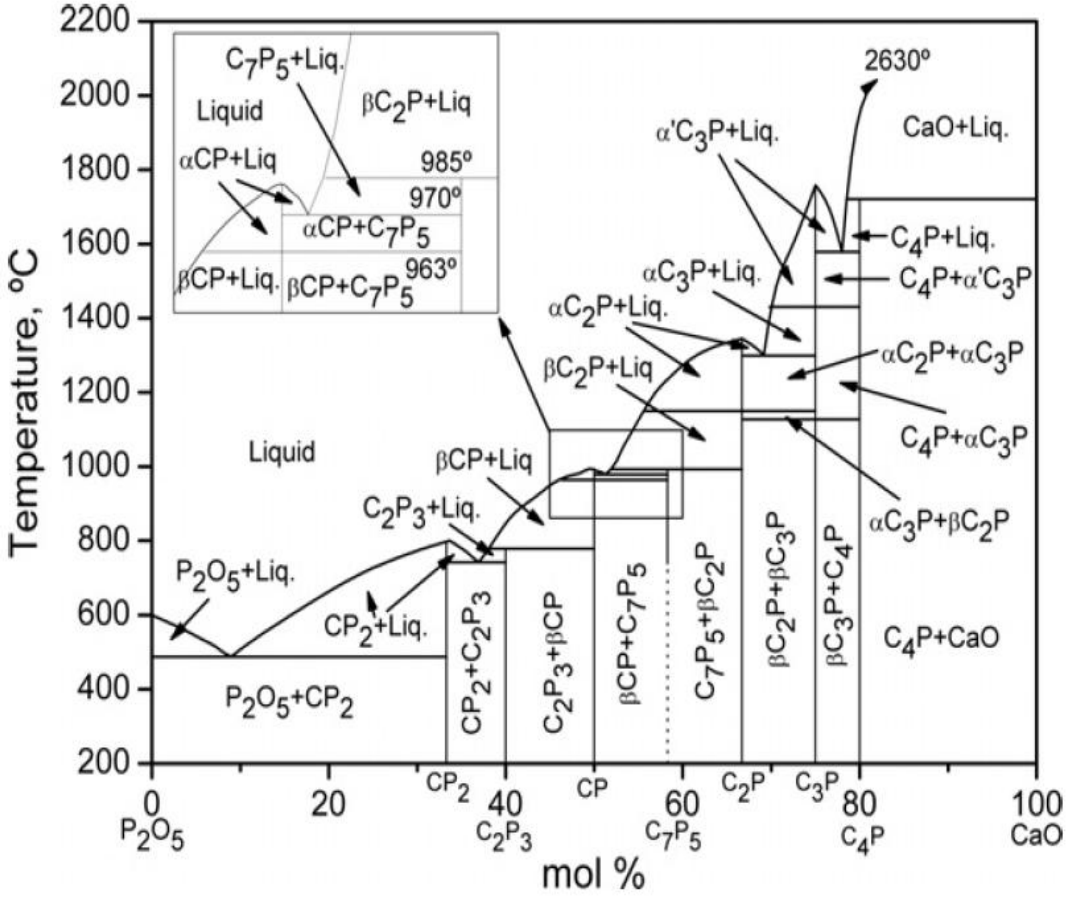

Figure 4: Phase diagram of CaO- P_2O_5 system [18].

As mentioned earlier, structural differences change solubility behavior and density of tricalcium phosphate. Basic building blocks of TCPs are Ca^{2+} cations and PO_4^{3-} anions arranged in two types of columns along [0 0 1] crystallographic direction; C-C representing cation-cation columns and C-A representing cation-anion columns. Each C-C column is surrounded by six C-A columns, and in turn, the C-A column is encircled by three C-C and three C-A columns to the total number of six. C-C columns are quite distorted from the straight line, as shown in Figure 5 on right [18][19].

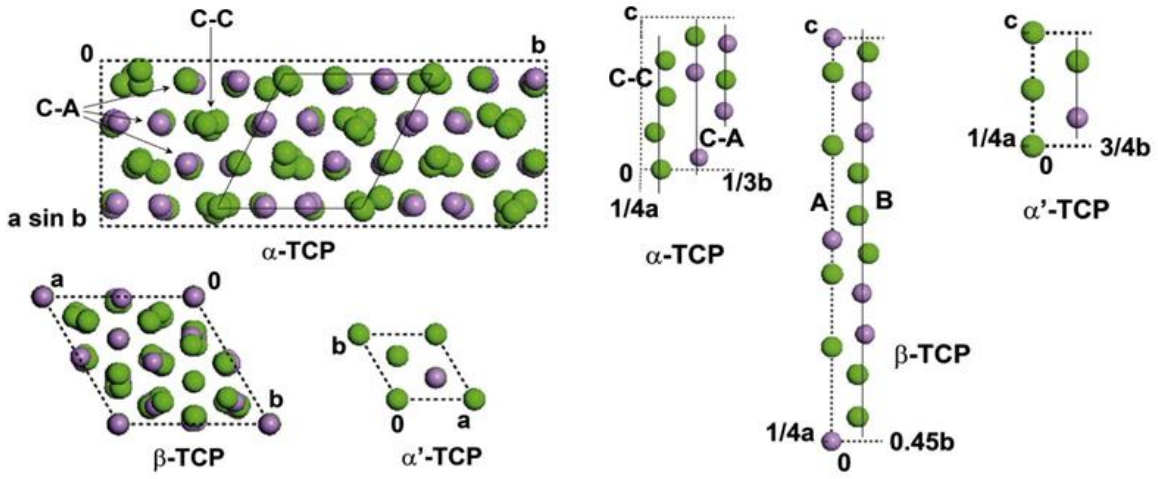

*Figure 5: Schematic representation of the projections of the α-TCP, β-TCP and α' -TCP unit cells along the [0 0 1] direction (**top view on left**) and fractional projections of the α-TCP, β-TCP and α' -TCP unit cells on the bc plane showing the disposition of constituent atoms in columns oriented along direction [0 0 1] (**edge on view on right**): Ca^{2+}, green; P^{5+}, magenta; O_2 has not been represented for the sake of clarity. C-C, cation–cation column; C-A, cation–anion column; A, A column; B, B column [18].*

β-phase shows presence of two distinct C-A columns, A columns comprised of -P-Ca-Ca-P- sequence and B columns with -P-Ca-Ca-Ca-P- sequence. Lack of C-C column in β- phase, and presence of A and B columns is responsible for differences in density and solubility due to better stacking of A and B columns. Therefore, β- phase is more densely packed meaning it possesses higher theoretical density, as seen in Table 1, which in turn decreases solubility and degradation rates in the physiological environment due to poor penetration of the solvent medium. The same logic can be applied vice versa for α-TCP [18].

Table 1: Structural data of TCP polymorphic modifications [20][21].

Property	$Ca_3(PO_4)_2$ polymorph		
	β-$Ca_3(PO_4)_2$	α-$Ca_3(PO_4)_2$	α′-$Ca_3(PO_4)_2$
Symmetry	Rhombohedral	Monoclinic	Hexagonal
Space group	*R3C*	$P2_1/a$	$P6_3/mmc$
a (nm)	1.04352(2)	1.2859(2)	0.53507(8)
b (nm)	1.04352(2)	2.7354(2)	0.53507(8)
c (nm)	3.74029(5)	1.5222(3)	0.7684(1)
α (°)	90	90	90
β (°)	90	126.35(1)	90
γ (°)	120	90	120
Z	21	24	1
V (nm^3)	3.5272(2)	4.31(6)	0.19052(8)
V_0 (nm^3)	0.1680(2)	0.180(6)	0.19052(8)
D_{th} ($g\,cm^{-3}$)	3.066	2.866	2.702

Structural characteristics of calcium phosphates are generally studied using X-ray diffraction analysis (XRD), Fourier transformed infrared spectroscopy (FTIR) and Raman infrared spectroscopy. More advanced methods e.g. neutron diffraction, X-ray absorption near edge surface spectroscopy (XANES) and even solid state ^{31}P magnetic-angle spinning nuclear magnetic resonance (MAS-NMR) can also be used to obtain specific structural data. XRD analysis in particular, is not only analytical method for determination of phase composition of TCP powder but can be also used to study setting properties of prepared cement by evaluating

conversion of α-TCP to hydroxyapatite (HA) or calcium deficient hydroxyapatite (CDHA) respectively. The Figure 6 below depicts the similarities and differences in XRD diffractograms of significant CP phases and HA [18][22].

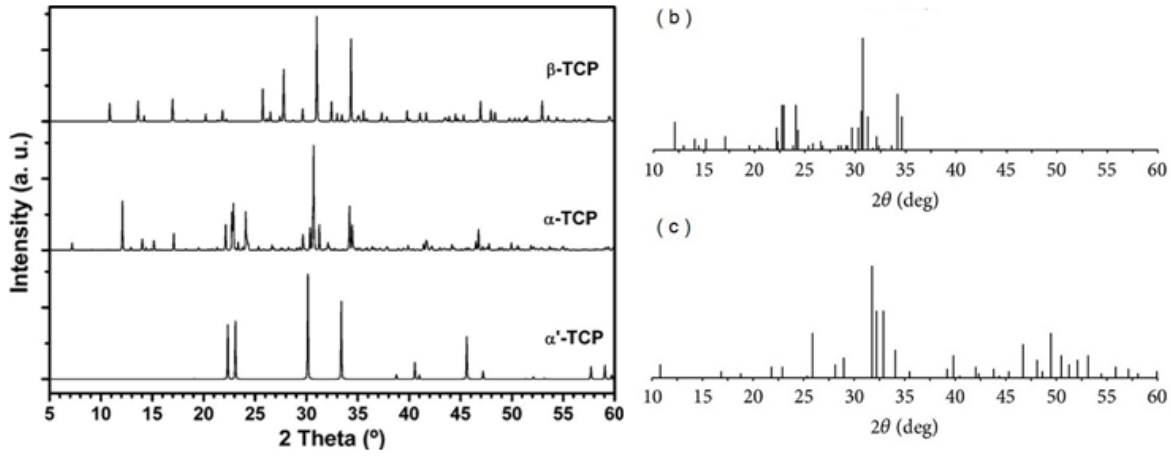

Figure 6: XRD diffractograms depicting major TCP phases and comparison between b) α-TCP, c) HA[18][22].

Changes in molecular shape e.g. symmetric or anti-symmetric stretchings and bendings of PO_4^{3-} group, which occur after exposing the sample to infrared radiation, are studied using FTIR and Raman spectroscopy. Data from FTIR and Raman analysis are shown in Table 2 [18][23].

Table 2: Main bands, their characteristic wavenumbers and intensities in IR and Raman spectra of TCPs [23].

Normal modes	Free PO_4^{3-} (cm^{-1})	α-TCP		β-TCP	
		IR (cm^{-1})	Raman (cm^{-1})	IR (cm^{-1})	Raman (cm^{-1})
Symmetric P–O stretching, ν_1	938	954 (s)	954 (w, sh)	972 (s)	948 (s)
			964 (s)	945 (s)	970 (s)
			976 (s)		
Symmetric P–O bending doubly degenerate, ν_2	420	415 (w)	421 (w)	419 (vw)	406 (m)
		430 (w)	451 (w)	438 (vw)	442 (m)
		454 (w)		458 (vw)	481 (m)
		463 (w)		497 (vw)	
		471 (w)			
Anti-symmetric P–O stretching triply degenerate, ν_3	1017	984 (s)	998 (s)	1025 (s)	1017 (w, br)
		997 (s)	1012 (w)	1044 (s)	1048 (vs)
		1013 (s)	1027 (w)	1066 (w, sh)	
		1025 (s)	1058 (w)	1083 (w, sh)	
		1039 (s)	1077 (w)		
		1055 (s)			
Anti-symmetric P–O bending triply degenerate, ν_4	567	551 (s)	563 (s)	544 (w, sh)	549 (w)
		563 (s)	577 (s)	555 (s)	573 (w)
		585 (s)	593 (s)	594 (w, sh)	547 (w)
		597 (s)	610 (s)	609 (s)	609 (w)
		613 (s)	620 (s)		

vs, very strong; s, strong; m, medium; w, weak; vw, very weak; sh, shoulder; br, broad.

2.3.2. Synthesis

Various synthetic routes are used to produce high-quality TCP powder, main of which include the thermal transformation of precursor with defined calcium to phosphorus ratio, solid-state synthesis from precursors, self-propagating high-temperature and combustion synthesis.

Thermal transformation technique makes use of previously obtained precursors e.g. CDHA, amorphous calcium phosphate (ACP), and β-TCP, prepared by various synthetic routes, to

thermally decompose to form an α-TCP powder. Generally speaking, for reaction to occur according to equations below, the Ca/P molar ratio should be adjusted to 1.5. Deviations in Ca/P molar ratio result in formation HA due to inappropriate stoichiometry [18]. CDHA decomposes to β-TCP at temperatures above 800 °C. Heating the sample to temperatures above 1200 °C results in decomposition of β- phase to α-TCP. According to Jokic, maximum transformation can be obtained by heating the sample to 1500 °C for 2 hours [24]. Equation 2 represents the thermal transformation of CDHA into α-TCP. In truth, equation 2 is reverse of setting reaction described in equation 1 mentioned above. Equation 3 describes the thermal decomposition of ACP forming α-TCP and water [18].

$$Ca_9(HPO_4)(PO_4)_5(OH) \rightarrow 3\ \alpha - Ca_3(PO_4)_2 + H_2O \quad T \geq 1150\ °C \tag{2}$$
$$Ca_9(PO_4)_6 \cdot n\ H_2O \rightarrow 3\ \alpha - Ca_3(PO_4)_2 + n\ H_2O \tag{3}$$

The solid-state reaction between solid precursors is the preferred synthetic route in literature reports. The synthesis is carried out obeying the general rules for solid-state reactions, i.e. solid precursors are milled together to reduce particle size, increase the contact area and mix them intimately. Wet milling is generally preferred. After milling, the mixture of powders may be directly heated above the transformation temperature or pressed to improve contact between particles. The recommended reaction temperatures varied between 1250 °C and 1500 °C, and the dwell time was between 2 and 48 h. Quenching of prepared powder is recommended to stabilize metastable α-TCP and avoid reversion back to to β- phase. Equations 4, 5, 6 and 7 below represent synthetic routes, possible reactants which can be used for powder preparation and obtained reaction products [18].

$$CaCO_3 + 2\ CaHPO_4 \rightarrow \alpha - Ca_3(PO_4)_2 + CO_2 + H_2O \tag{4}$$
$$3\ CaCO_3 + 2\ NH_4H_2PO_4 \rightarrow \alpha - Ca_3(PO_4)_2 + 3\ CO_2 + 3\ H_2O + 2\ NH_3 \tag{5}$$
$$CaCO_3 + Ca_2P_2O_7 \rightarrow \alpha - Ca_3(PO_4)_2 + CO_2 \tag{6}$$
$$Ca_{10}(PO_4)_6(OH)_2 + 2\ CaHPO_4 \rightarrow 4\ \alpha - Ca_3(PO_4)_2 + 2\ H_2O \tag{7}$$

Self-propagating high-temperature synthesis, as well as combustion synthesis, have also been employed as powder preparation techniques. For self-propagating synthesis high-temp. synthesis, pellets containing a mixture of CaO and P_2O_5 powders in ratio 3:1 are prepared and reacted in an argon atmosphere. Heat is provided by tungsten filament which heats sample until the point of ignition at the bottom of pellet, initiating reaction, ultimately producing α-TCP. Unfortunately, this method produces α-TCP powder containing significant amounts of HA and β-TCP [25]. For combustion synthesis, a solution containing oxidizing agents (nitrates), soluble calcium and phosphate salts with required Ca/P ratio and organic fuel such as urea is burned forming desired powder product with a small particle size [26].

Introducing various ionic substituents results in change of thermodynamic relation between α- and β- phases. Partial substitution of Ca by Mg, Sr or Zn cations increases the thermal stability of β-TCP. In the interest of producing more pure α-TCP, such impurities have to be removed [22][23]. Alternatively, partially substituting PO_4 for SiO_4 stabilizes α-phase. Thus, doping with silicates has been employed to produce pure α-TCP [29].

2.3.3. Solubility, pH and biodegradability

As was discussed earlier, structural differences between α- and β- phases of TCP are closely linked to differences in solubility, density, and biodegradability. In general, lower the Ca/P ratio, more acidic and soluble the calcium phosphate is, this logic can be applied vice versa. Some of the listed calcium phosphates in Table 3 are brushite – dicalcium phosphate dihydrate (DCPD, $CaHPO_4 \cdot 2H_2O$), monetite – anhydrous dicalcium phosphate (DCPA,

$CaHPO_4$), octacalcium phosphate (OCP, $Ca_8(HPO_4)_2(PO_4)_4 \cdot 5H_2O$), α-TCP (α-$Ca_3(PO_4)_2$), β-TCP (β -$Ca_3(PO_4)_2$), HA ($Ca_{10}(PO_4)_6(OH)_2$) and tetracalcium phosphate (TTCP, $Ca_4(PO_4)_2O$) [30].

Table 3: Solubility table of selected calcium phosphates [30].

Ca/P	Compound	$-\log K_{ps}$		Solubility (mg L^{-1})	
		25 °C	37 °C	25 °C	37 °C
1.0	$CaHPO_4 \cdot 2H_2O$	6.59	6.73	87	74
1.0	$CaHPO_4$	6.90	7.04	48	41
1.33	$Ca_8(HPO_4)_2(PO_4)_4 \cdot 5H_2O$	96.6	98.6	0.025	0.018
1.5	α-$Ca_3(PO_4)_2$	25.5	28.5	0.97	0.24
1.5	β-$Ca_3(PO_4)_2$	28.9	29.6	0.20	0.15
1.67	$Ca_{10}(PO_4)_6(OH)_2$	116.8	117.2	0.00010	0.000096
2.0	$Ca_4(PO_4)_2O$	38–44	37–42	0.28–0.038	0.39–0.075

At physiological conditions of 37 °C and pH of 7.2 – 7.4, the concentration of dissolved Ca and P species decreases in the order displayed in equation 8. This means, that at given conditions, HA is a most stable polymorphic modification, therefore exists as a desired final product of cement setting reaction [18].

$$\text{TTCP} > \alpha - \text{TCP} > DCPD > DCPA > OCP > \beta - \text{TCP} > HA \quad (8)$$

2.4. Cement additives

Even though CPCs are suitable for bone repair and bone regeneration applications, we are still dealing with bioceramics, which are infamously known for their brittleness. To get around this fact, a variety of additives are incorporated into cement to improve the performance of such material. Additives are mainly used to improve the strength of the material by introducing reinforcements into cement structure, the morphology of prepared cement e.g. porosity modifiers. Rheological attributes can be adjusted to ensure the injectability of cement paste, and the addition of antibiotics can diminish possible inflammatory reaction. Other additives worth mentioning are growth directing polymer coatings enhancing cell growth on CPC surface.

2.4.1. Fiber reinforcements

Brittleness is a major drawback of CPCs; cements mechanical properties are due to lack of organic collagen phase inferior to native bone. The main cause for this brittleness is their low resistance to crack propagation, which ultimately leads to catastrophic failure. The addition of stiff and strong fibers for mechanical reinforcement of CPCs has become increasingly popular. This way, loads can be transferred from the brittle matrix to the fibers, thereby improving the toughness and ductility of the resulting composite by mechanisms such as crack deflection, fiber bridging, and frictional sliding. Reinforcement can be provided by inorganic e.g. carbon fibers or synthetic polymer fibers. Synthetic polymer fibers can be divided further into non-resorbable and resorbable reinforcements, where resorbable fibers are more advantageous for they can be “tailor-made” for application by adjusting the length of fiber, strength, and most importantly their biodegradability. However, the challenge is the incorporation of long fibers into CPCs in a homogeneous manner, therefore shorter fibers are preferable [31][34].

Non-resorbable fibers are represented by carbon fibers, carbon nanotubes, and non-degradable polymer fibers such as polyaramides and polyamides. Carbon fibers have been used as reinforcers in composite materials to provide them with high compression and tensile strength, as well as stiffness. Studies show, that carbon fibers do not interfere with TCP setting and fibers integrate into matrix reasonably well, which increases material's mechanical parameters [44]. Carbon nanotubes (CNTs), comprised of rolled-up graphene sheets with hemispherical half-fullerene endcaps, were also investigated as potential reinforcing agents. Mineralization of CNTs with HA and functionalization of CNTs with –OH, –COOH functional groups showed even better interfacial bonding to the matrix, resulting in a significant increase in mechanical properties [45][46].

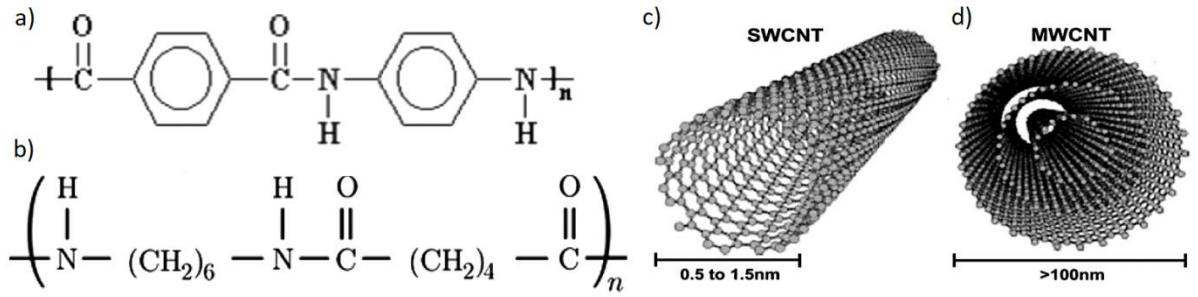

Figure 7: Structures of non-degradable reinforcements: a) para-polyaramide (top), b) polyamide PA6.6 (bottom), c) single-walled carbon nanotube, d) multi-walled carbon nanotube [34][47].

Fibers made from para-polyaramide also known by its commercial name Kevlar were investigated as well. Kevlar is notoriously known for its high elastic modulus and high resistance. Unfortunately, exceptional properties of these fibers make them quite expensive. Unparalleled mechanical parameters of fibers demonstrably proven, that out of all the reinforcing agents, p-polyaramide fiber composites perform the best [44]. Cheaper alternative for polyaramides are polyamides, drawbacks are their inferior mechanical properties. But the biggest disadvantage of non-resorbable fibers is precisely their non-resorbability. The addition of non-resorbable fibers into resorbable cement matrices would result in fiber release to the surrounding tissues, with the subsequent biocompatibility risks. The most critical case would be for CNTs due to their nanometer scale [34].

Resorbable polymer fibers used in fiber reinforced CPC composites belong to the family of polyesters; polymer chain contains ester functional group emerging from the reaction of a hydroxyl group of alcohol with a carboxylic acid group. These polyesters are insoluble in water but they can degrade by the hydrolytic attack of the ester bond. Most commonly used polymer fiber reinforcements are made from poly(*levus*-lactic acid) or PLLA, poly(lactic-co-glycolic acid) or PLGA, and poly(ε-caprolactone) or PCL.

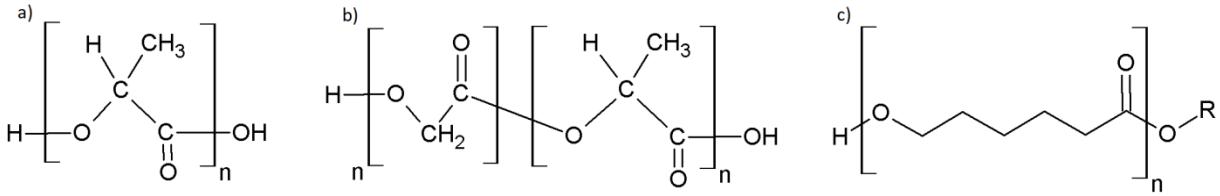

Figure 8: Chemical structures of biodegradable polymer reinforcements: a) PLLA, b) PLGA, c) PCL [34][35].

All of the mentioned polymer fibers are produced using electrospinning or centrifugal (force) spinning. Fiber diameter is adjusted using different production (spinning) method, concentrations of solution prior to electro spinning, and acceleration voltage. Centrifugal

spinning produces fibers with micrometer sized diameter fibers. High voltage electrospinning is capable of producing ultrafine nano-scale fibers in form of bundles. These tangled bundles are then ground or cut to desired sizes and added to cement composition [32][33][34].

Biodegradability of these particular polymers is dependent on polymer crystallinity and molecular weights. PLGA shows fastest degradation rates of the latter. Variations in the molar ratio between constituents – poly(glycolic acid) and poly(lactic acid), are used for tuning the rate of biodegradability. Therefore, PLGA is mainly used as short term CPC reinforcement and can be used as porosity modifier to increase the total porosity of CPC [34][36]. On the other hand, poly(ε-caprolactone) (PCL) has the lowest degradation rates; it degrades almost three times slower than poly(*levus*-lactic acid) (PLLA) [36]. Hence, PCL is used as a long term reinforcement and PLLA stands on a middle ground between long and short term reinforcements. To accommodate for the better reinforcing effect, different weight percentages of fibers can be used, and consecutively certain mechanical properties of the material can be improved to some extent. Modification of fibers using triblock copolymer based on poly(ethylene glycol) and poly(propylene glycol) (PEG-PPG-PEG) commercially known as Pluronic or Poloxamer, can be also used to improve wetting of fibers. Pluronic molecules are amphiphilic; polymer contains both hydrophobic and hydrophilic properties. This fact can be exploited for better incorporation of hydrophobic fibers into matrix resulting in improvement of reinforcement capabilities of fibers. Sadly, Pluronic is non-degradable, only water-soluble and exhibits toxicity at higher concentrations [38][48].

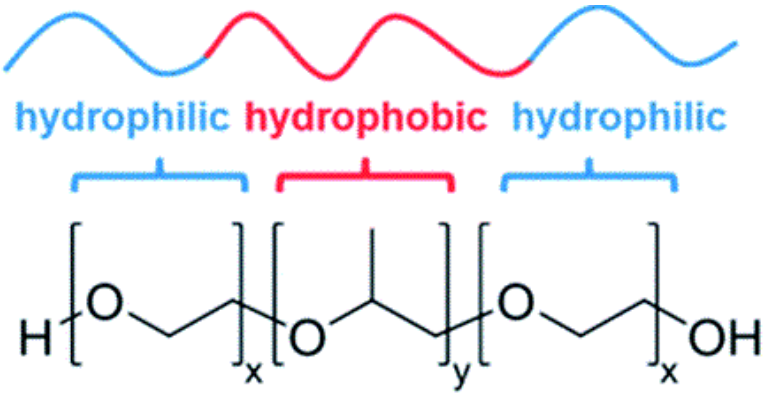

Figure 9: Schematic of PEG-PPG-PEG copolymer showing hydrophilic and hydrophobic constituents [50].

On the other hand, introduction of degradable reinforcement into CPC is a double-edged sword, has its advantages but also disadvantages. Reports show, that addition of fibers positively influences flexibility, and work on fracture, rendering final CPC more resistant to fracture and crack propagation. Degradation of fibers over time increases material's porosity, which is desirable for bone regeneration [34]. Pores formed like this are interconnected, which is advantageous for the ingrowth of new bone, especially in long-term tissue interface maintenance. However, materials containing interconnective pores are less able to contain osteogenic cells, resulting in a longer period until the pore space has been filled with newly formed bone [37]. While higher bone regeneration capabilities are desirable, due to increased porosity mechanical properties are negatively affected. Long fibers may significantly alter rheological aspects of CPC paste. This can cause trouble with cement's injectability. Hydrophobicity of fibers themselves presents a challenge due to their poor integration and adhesion to calcium phosphate matrix. Also, unmodified fiber's hydrophobicity results in undesirable clumping of fibers. This is the main contributor of fiber inhomogeneity in CPCs. These challenges have to be tackled to ensure composite's best performance [34].

2.4.2. Structural and rheological modification

As mentioned earlier, porosity is an important factor to consider when dealing with osteointegration and consecutive bone regeneration. Desired morphology of CPC can be also achieved using suitable additives, also known as porogens. One of many candidates is sodium hydrogen carbonate, otherwise known as baking soda – $NaHCO_3$. $NaHCO_3$ in small weight percentage is homogenized in a powder phase of cement and instead of pure water, a slightly acidic aqueous solution of monosodium phosphate (NaH_2PO_4) functions as the liquid phase. Mixing of the components initiates decomposition of sodium bicarbonate to CO_2 which creates bubbles, forming voids and pores [41].

Another way to create pores is a mechanical route; creation of pores while mixing. Thorough mixing or whipping of the cement paste with appropriate tool introduces bubbles of air into the paste which cannot escape once paste has solidified. Unfortunately, drawbacks for these methods are the same; pores diminish mechanical parameters and therefore affect the final performance of the material.

To perform a minimum invasive surgery, cement paste requires also a good degree of injectability. As soon as the water is added to α-TCP powder setting reaction starts, and workability of paste gradually decreases. Supplementing CPC with polymeric additives appears as a promising strategy to tune injectability of the paste. Variety of additives have been investigated, namely hydrogels based on collagen, gelatin, carboxymethylcellulose, hyaluronic acid, chitosan, synthetic PEG and many others. For its thermo-responsive behavior and washout resistance, already mentioned Pluronic has been investigated as well. Drawbacks already mentioned are its non-degradability and toxicity [38][49]. Addition of biodegradable and thermosensitive copolymer similar to PEG-PPG-PEG, but based on hydrophobic poly(lactic acid), and poly(glycolic acid) as well as hydrophilic poly(ethylene glycol) (PLGA-PEG-PLGA) triblock copolymer, is proposed as an alternative solution to control paste's injectability. PLGA-PEG-PLGA copolymer exists as a free-flowing solution at room temperature and undergoes gelation at physiological conditions to a three-dimensional network, the so-called hydrogel. This fact can be used in combination with TCPs to enhance injectability due to advantageous thixotropic behavior of copolymer with prepared CPC paste. Another useful advantage of triblock copolymer is its non-toxicity, and complete biodegradability; copolymer is fully degradable in Krebs cycle to its acidic constituents and subsequently to carbon dioxide and water [38][39].

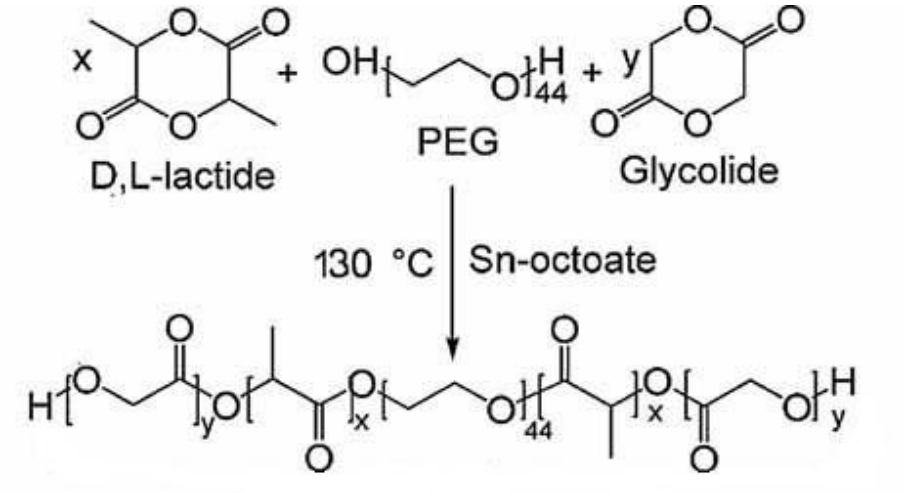

Figure 10: Reaction schematic of PLGA-PEG-PLGA copolymer synthesis [40].

The PLGA-PEG-PLGA triblock copolymer was prepared via conventional ring-opening polymerization (ROP) method in a bulk under nitrogen atmosphere. Poly(ethyleneglycol) (4 mmol), lactide (83 mmol) and glycolide (28 mmol) were homogenized at 130 °C followed by injecting tin octanoate (Sn^{2+} bis(2-ethylhexanoate)) (0.1 mmol). Reaction proceeded for 3 hours. Product was purified from unreacted monomers by dissolving in cold water and heating the solution up to 80 °C. Precipitated polymer was separated by decantation and dried in vacuum oven at 30 °C until the constant weight [40].

2.4.3. Anti-inflammatory agents and polymer coatings

In order for the material to function as a drug carrier, it must possess the ability to incorporate a drug either physically or chemically, retain the drug until it reaches the specific target site, and gradually deliver the drug to affected tissue in a controlled manner over time. Fortunately, all of these criteria are well met by CPCs [42].

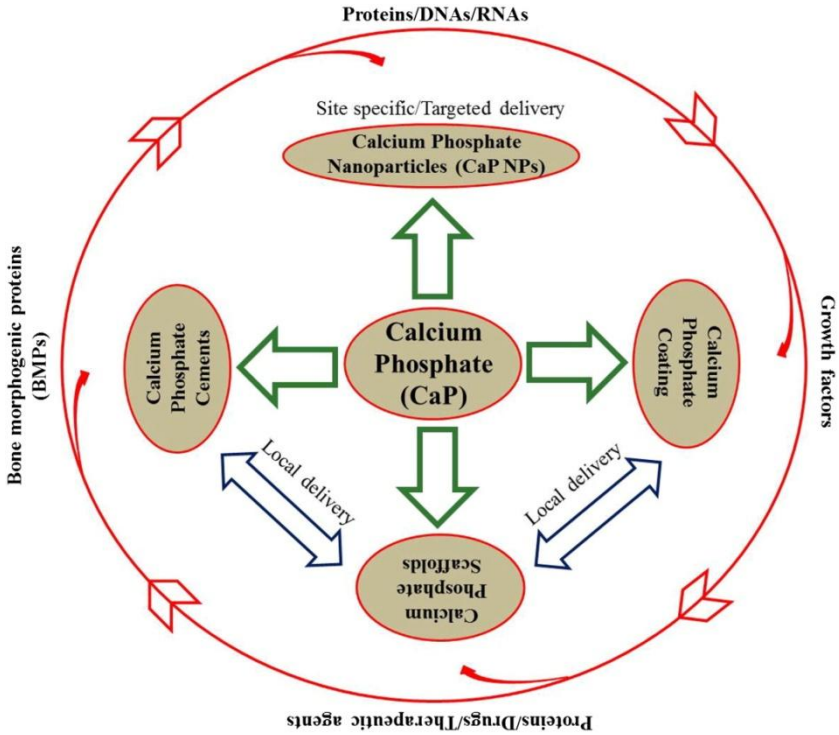

Figure 11: Various application approaches of CPCs [42].

In addition to acting as an appropriate bone substitute, CPCs can also be used for local drug delivery for treatment of different skeletal diseases such as bone tumors, osteoporosis, and osteomyelitis. The porous structure of CPC functions as a vessel for drugs, which are gradually released during material's degradation. Treatment of osteomyelitis in particular is provided via incorporation of antibiotics such as vancomycin, and gentamicin into cement. These antibiotics are currently used for treatment of musculoskeletal disorders. Alas, it has been reported that incorporation of vancomycin in higher concentrations influences composite mechanical parameters, and decreases compressive strength of CPC composite [42][43].

Polymer coatings have long been recognized as a powerful tool to control and steer cell responses – adhesion, proliferation, and differentiation. Use of polydopamine (PDA) proposes a novel approach of forming such a layer via oxidative self-polymerization of dopamine at slightly basic conditions. This layer is responsible for better adhesion of cells to the surface while secondarily increasing photoprotection and metal cation sequestering [51].

2.5. Applications of calcium phosphate cements

Biodegradable bone cements have significant potential with respect to the fields of dentistry, craniofacial and maxillofacial surgery, orthopedics, traumatology, vertebroplasty, and kyphoplasty procedures as well as drug carriers. Advantageous properties e.g. biocompatibility, bioactivity, osteoconductivity, mouldability of paste and nontoxicity make them perfect candidates for mentioned applications [52].

The use of CPCs for craniofacial applications seems logical, as there is little or no stress generated under these conditions. Moreover, the ability to mold the material at placement is an enormous advantage from a cosmetics standpoint. Commercially available product BoneSource™ has been successfully employed in craniofacial applications. The product is based precisely on calcium phosphates which undergo transformation into HA [53]. In stomatological applications, CPCs were tried as root canal fillers and for pulp capping [54]. Distal radius fractures, hip fractures, tibial plateau fractures, and many other bone complications were successfully treated with CPCs. Vertebroplasty and kyphoplasty are two surgical procedures that recently have been introduced to medically manage of osteoporosis-induced vertebral compression fractures. Particularly, both procedures aim to augment the weakened vertebral body, stabilize it and/or restore it to as much of its normal height and functional state as possible. Both procedures involve the injection of a self-setting paste of calcium orthophosphate cement into the fractured vertebral body, which resulted in faster healing [52].

As seen in this short review, properly modified calcium phosphate bone cement finds many uses in today's clinical applications. Therefore, improving the properties even further and looking for more novel strategies to enhance the paste's performance is a viable strategy for future research.

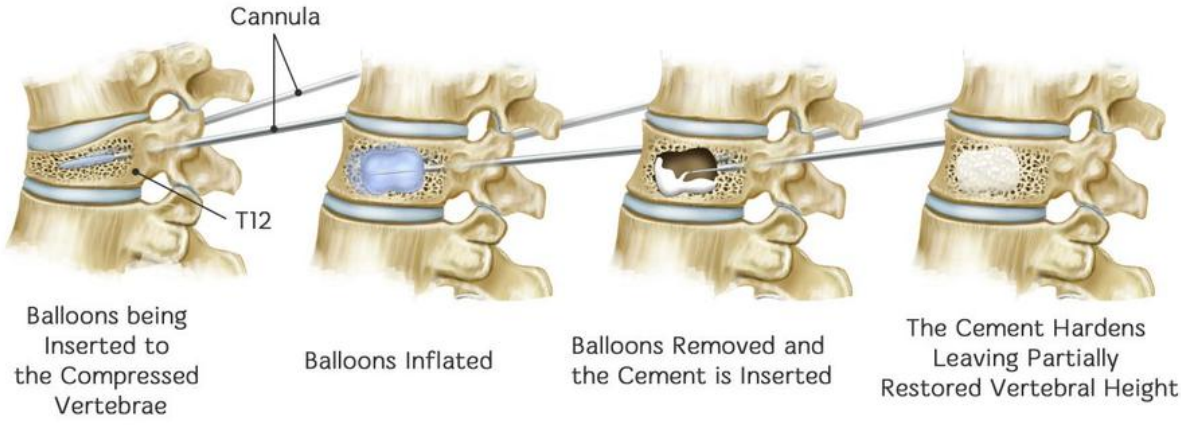

Figure 12: Schematic of kyphoplasty procedure [57].

3. GOAL OF THE WORK

The aim of this thesis is to verify if the addition of biodegradable polymer fiber reinforcements positively influences mechanical properties of porous cement pastes without negatively affecting rheology which is closely linked to paste's injectability.

The novelty of work resides mainly in use of biodegradable polymer fibers in conjunction with biodegradable, thixotropic, and thermosensitive PLGA-PEG-PLGA copolymer used to enhance injectability of paste. Degradation of the mentioned copolymer, as well as thorough mixing of cement paste during sample preparation, introduces pores into cement's structure, improving its osteoconductivity. Nonetheless, pores and voids diminish the mechanical properties of cement. Therefore, the use of degradable reinforcements based on PCL and Pluronic modified PCL fibers, is proposed as a solution to weak mechanical properties.

The thesis deals with:

- a literature review of polymer fiber reinforced calcium phosphate bone cements
- synthesis and characterization of cement constituents i.e. α-TCP powder, PLGA-PEG-PLGA copolymer, and reinforcing PCL and Pluronic modified PCL fibers
- preparation of cement samples with various degrees of porosity and fiber content
- analysis of mechanical, rheological, structural and morphological properties of cement samples
- evaluation of reinforcing, setting and rheological behavior of cement pastes, comparisons of sample performances
- elaboration of obtained data, and devising optimal fiber content for bone cement application

The outcome of the work should bring a better understanding of reinforcing capabilities of PCL and modified PCL fibers. Due to use of reinforcements, results are expected to show certain improvement of cement strength in compression and tensile domain; decrease in cement brittleness. These factors are the main driving force for the topic of the thesis as well as further research, and implementation of this particular cement into surgical practice.

4. EXPERIMENTAL PART

4.1. Chemicals

- Poly(ethyleneglycol) (PEG M_w = 1500 g·mol^{-1}) supplied by Fluka (Switzerland)
- Glycolide (GA ≥99.9 %) purchased from Polysciences (PA, USA)
- D,L-Lactide (LA ≥99.9 %) purchased from Polysciences (PA, USA)
- Tin octanoate (Sn^{II} 2-ethylhexanoate 95 %) supplied by Sigma-Aldrich (MO, USA)
- Calcium carbonate ($CaCO_3$ ≥99%) supplied by Sigma-Aldrich (MO, USA)
- Calcium hydrogen phosphate ($CaHPO_4$ ≥98%) supplied by Sigma-Aldrich (MO,USA)
- Poly(ε-caprolactone) (M_w = 45000 g·mol^{-1}) supplied by Sigma-Aldrich (MO, USA)
- Poloxamer 188, commercial name Pluronic® F-68 (M_w = 8350 g·mol^{-1}) supplied by Sigma-Aldrich (MO, USA)
- Chloroform supplied by Merck (NY, USA)
- Ethanol (96%) supplied by Merck (NY, USA)
- Isopropyl alcohol supplied by VWR (Austria)
- Ultrapure water (Type I H_2O according to ISO3696)
- Liquid nitrogen (LINDE company, Brno)

4.2. Equipment

- OHAUS Adventurer Pro, analytical Balance (Germany)
- HIRSCHMANN Labopette 1000 µl, micropipette (Germany)
- MERCK Direct-Q 3 UV, ultrapure water purification system (MA, USA)
- CHRIST Epsilon 2-10D LSCplus, lyophilizator (Germany)
- XENOX Roti, speed-stirring mixer (Germany)
- MMM GROUP CO2cell 50, laboratory incubator (Germany)
- SICCO Star-Desiccator, cabinet desiccator (Germany)
- HORIBA LA-950, laser scattering particle size distribution analyzer (Japan)
- AGILENT 1260 Infinity, liquid chromatograph (HPLC GPC/SEC) (CA, USA)
- RIGAKU MiniFlex 600, X-ray diffractometer (Japan)
- BRUKER Hyperion3000/Vertex 70V, FTIR spectrometer (Germany)
- INSTRON 8874 bi-axial tabletop servohydraulic testing system 25 kN/100 Nm (UK)
- LEICA EM ACE600, sputter coater (Germany)
- TESCAN MIRA3 XMU, scanning electron microscope (Czech republic)
- BRUKER GE phoenix v|tome|x L240, micro-computed tomograph (Germany)
- TA INSTRUMENTS ARES-G2, rotational rheometer (DE, USA)

4.3. Synthesis of input materials

4.3.1. PLGA-PEG-PLGA thermosensitive copolymer

Thermosensitive PLGA-PEG-PLGA copolymer was prepared according to article by Michlovská et. al. Reaction schematic can be found in Figure 10 [40]. The obtained crude copolymer was purified by water. After being completely dissolved, the polymer solution was heated to 80 °C to precipitate the polymer product and remove water-soluble low-molecular weight polymer and unreacted monomers. The purification process was repeated three times. The residual water in the precipitated copolymer was left over night in lyophilizator at –70 °C and freeze dried until the constant weight.

4.3.2. α-tricalcium phosphate powder

α- phase of tricalcium phosphate powder used in experiments was synthesized via conventional solid state synthesis at 1400 °C from $CaCO_3$ and $CaHPO_4$ precursors. Ratio of $CaCO_3$ to anhydrous $CaHPO_4$ was adjusted to 2:1. Air quenching was used to prevent transformation of α- to β- phase. Obtained block was dry milled in planetary mill for 15 minutes at 450 rpm. Powder was then sieved for 30 minutes using 40 μm sieves [38].

4.3.3. PCL and PCL-Pluronic modified reinforcing fibers

Polymer fibers were supplied by InoCure l.t.d. The short fibers were prepared using modified wet electrospinning technology on InoSpin device. PCL in 20 wt. % and Pluronic F-68 in 1 wt. % were dissolved in mixture of chloroform:ethanol (9:1) until homogeneous solution was obtained. Wet electrospinning apparatus (InoSPIN, InoCure) consisted of needle electrode (Gauge 20) delivering the polymeric solution (0.15 ml/min) and wet collector. Wet collector was made of isopropyl alcohol stirred bath (400 rpm) which was grounded. Needle was connected to high voltage power supply generating electrostatic field with 30 kV potential. The distance between collector and electrode was 10 cm. The formed fluffy bundles of fibers were cut to short clumps using ultrasound (5 min, 75%, Misonix ultrasonic homogenizer) and the resulting dispersion was sieved using 250 μm analytical sieve (Spartan, FRITSCH sieve shaker). The short fibers were collected using vacuum filtration to 0.48 μm membrane (Millipore). Sterilization was performed using 20 min irradiation by UV light.

4.4. Sample preparation

At first, PLGA-PEG-PLGA copolymer was dissolved in ultrapure water with weight percentage concentration of 15 %. Ultrapure water was used to prevent other additives to interact with setting mechanisms. To avoid the formation of a hydrogel, which occurs at elevated temperatures, dissolution was carried out in the refrigerator at 4 °C. Homogeneity of the liquid phase was ensured using magnetic stirrer for at least three days. Completely dissolved polymer was afterwards ready to use. Liquid to powder ratio, L/P, was determined to be 0.5. This means, for every gram of liquid phase, twice as much powder was used. Powder phase was weighed on analytical balance, the same applied to fiber reinforcements. During the experiments, different weight percentages of reinforcing fibers were used to evaluate their reinforcing effect. Addition of fibers has been adjusted to the total mass of cement paste. Fibers were at first manually homogenized in a liquid phase, and then the rest of the powdered α-TCP was added and thoroughly mixed by spatula – dense samples, or using the XENOX Roti speed-stirring mixer – porous samples, for 1 minute totally. Prepared cement paste was consecutively transferred to 5 ml syringe and injected to 6×11 mm, 6×2 mm or 10×4 mm molds secured in silicone mold on Petri dishes. Prepared samples were readily transferred into incubator warmed to 37 °C equipped with a tray filled with demineralized water and covered up with glass water bath dish. After completing setting in the incubator, samples were removed from the incubator and their molds, optionally sandpapered to desired dimensions, and analyzed using methods below.

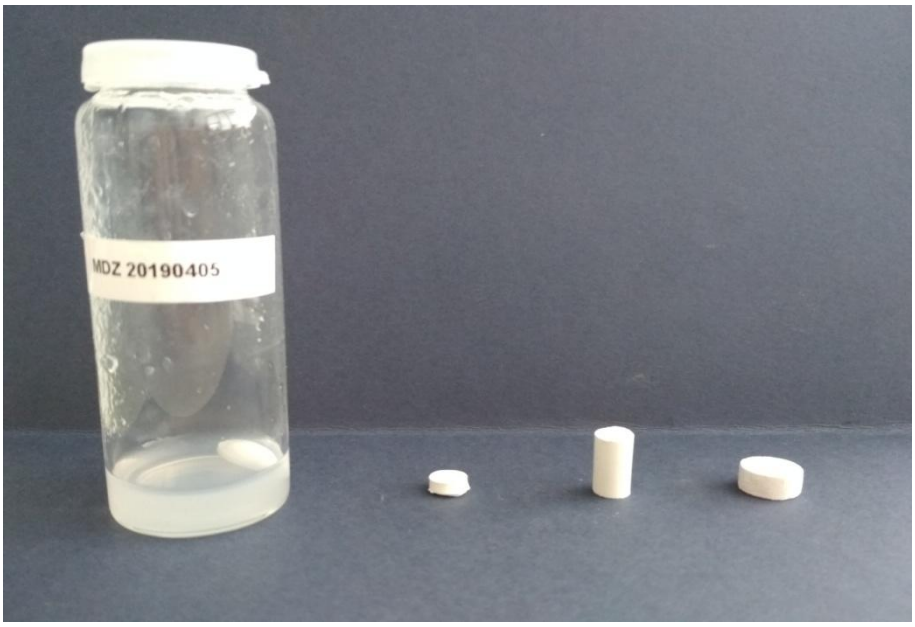

Figure 13: Image of prepared copolymer solution and samples with different dimensions.

4.5. Description of samples

Master's thesis deals with different cement compositions, types of fibers and mixing techniques. In the experiments, denomination dense and porous is used for differences in porosity. Dense samples were mixed with spatula whereas porous samples were mixed with XENOX Roti speed-stirrer. Different types of fibers and fiber contents were used for sample preparation. Description of said samples is specified in Table 6.

Table 4: Description of samples.

Sample Number	Sample Description	Sample labeling
1	Spatula mixed control sample	Dense control
2	Spatula mixed sample + 1 wt. % PCL-PLU	Dense PCL-PLU 1
3	Spatula mixed sample + 1 wt. % PCL	Dense PCL 1
4	Speed-stirred control sample	Porous control
5	Speed-stirred sample + 1 wt. % PCL-PLU	Porous PCL-PLU 1
6	Speed-stirred sample + 3 wt. % PCL-PLU	Porous PCL-PLU 3
7	Speed-stirred sample + 5 wt. % PCL-PLU	Porous PCL-PLU 5
8	Speed-stirred sample + 1 wt. % PCL	Porous PCL 1
9	Speed-stirred sample + 3 wt. % PCL	Porous PCL 3
10	Speed-stirred sample + 5 wt. % PCL	Porous PCL 5

4.6. Sample characterization

4.6.1. X-ray diffraction analysis

The hardened sample was removed from the mold and ground with a pestle in a ceramic mortar to fine powder. The powdered sample was spread on a glass sample holder in an even manner and inserted into a sample slot in RIGAKU MiniFlex 600 X-ray diffractometer. The analysis was conducted from 5 to 50 ° 2θ at a maximum of 40 kV of voltage and 15 mA of current. Obtained data were used to establish mineralogical and crystalline compositions of samples, as well as the transformation kinetics of α-TCP to CDHA and HA respectively.

4.6.2. Fourier-transform infrared spectroscopy

Ground sample was placed on an ATR crystal of BRUKER Hyperion3000/Vertex 70V FTIR spectrometer and secured using torque screw. Sample compartment was evacuated and analysis was conducted using MIR ATR (mid-infrared attenuated total reflectance) method with 4 cm^{-1} resolution, scanning time of 32 and range from 4500 to 800 cm^{-1}. FTIR spectra were used mainly to confirm the presence of polymer fibers in sample.

4.6.3. Mechanical analysis

Samples for mechanical testing were removed from mold and sandpapered to obtain smooth and parallel surfaces. Afterward, samples were measured using caliper ruler to establish sample dimensions. Next, the prepared sample was placed onto a compression testing device and measurement was started. Loading rates of 1 mm/min were used for compressive strength analysis; 0.5 mm/min was used for diametric tensile strength measurements. In total, 5 testing samples were tested and values were averaged to increase the reliability of measurement. Data from measurements e.g. compressive strengths, elastic moduli and diametric tensile strengths were calculated and stress-strain curves were produced.

4.6.4. Scanning electron microscopy

Samples for scanning electron microscopy were roughly ground in a ceramic mortar with pestle while submerged in liquid nitrogen. Ground samples were then transferred onto a SEM target equipped with carbon tape. Before measurement, samples were coated with thin layer of graphite enabling the charge to escape from sample. Measurement was done on TESCAN MIRA3 XMU scanning electron microscope with acceleration voltage ranging from 5 kV to 10 kV. Secondary electron (SE), and backscattered electron (BSE) detectors were used. SEM analysis provided morphological information about samples structure with an emphasis on fibers in the cement matrix.

4.6.5. Micro-computed tomography

Samples with dimensions of 6×2 mm were mounted into scanning chamber, and analyzed with X-ray tomograph. Resolution was set to 8 μm. Analysis provided 3-D image of sample, images of cross sections were exported and using ImageJ software pore size distribution was calculated.

4.6.6. Dynamic rheological analysis

Samples for rheological testing were prepared on spot before measurement the same way as described in the sample preparation section. TA INSTRUMENTS ARES-G2 rotational rheometer was prepared for measurement and equipped with plate-plate geometry and Peltier plate for temperature control. Measurement gap was set to 1000 μm. Distilled water was added into the top plate solvent trap reservoir to prevent drying of the sample during measurement. Bone cement sample was placed onto a Peltier plate and secured in place using top plate geometry. Excess material was removed using a spatula. Analyses were conducted for 1 hour at a temperature of 23 °C and 4 hours for 37 °C. Analysis at 23 °C was used to establish workability of paste and analysis at 37 °C provided data about paste's setting in physiological conditions.

5. RESULTS AND DISCUSSION

5.1. Characterization of input materials

5.1.1. PLGA-PEG-PLGA thermosensitive copolymer

Prepared and purified polymer was analyzed using gel permeation chromatography and dynamical rheological analysis. Number-average molecular weights were found to be equal to 5600 $g \cdot mol^{-1}$ and index of polydispersity (PDI = M_w/M_n) to 1.094 respectively. PDI value is quite close to 1 which represents quite narrow molecular weight distribution. Overview of exact values, as well as standard deviations from two trail runs, is shown in Table 4.

Table 5: Molecular weight and polydispersity indices of PLGA-PEG-PLGA copolymer obtained from gel permeation chromatography.

	Mn	PDI
Trial run 1	5.63×10^3	1.092
Trial run 2	5.60×10^3	1.096

Sol-gel transition data were obtained from the rheological analysis. Storage (G´) and loss (G´´) modulus versus temperature plot is depicted in Figure 14. Two significant crossovers of curves have been observed. The first crossover was found at 33 °C, and the second crossover at 40 °C. This means that the polymer solution increases its viscosity at 33 °C, which can be interpreted as a formation of "flower-like" micelles which form the hydrogel. At higher temperatures above 40 °C, phase-separation, and dehydration of micelles occurs. Hence two phase transitions, sol-to-gel, and gel-to-sol occur [38].

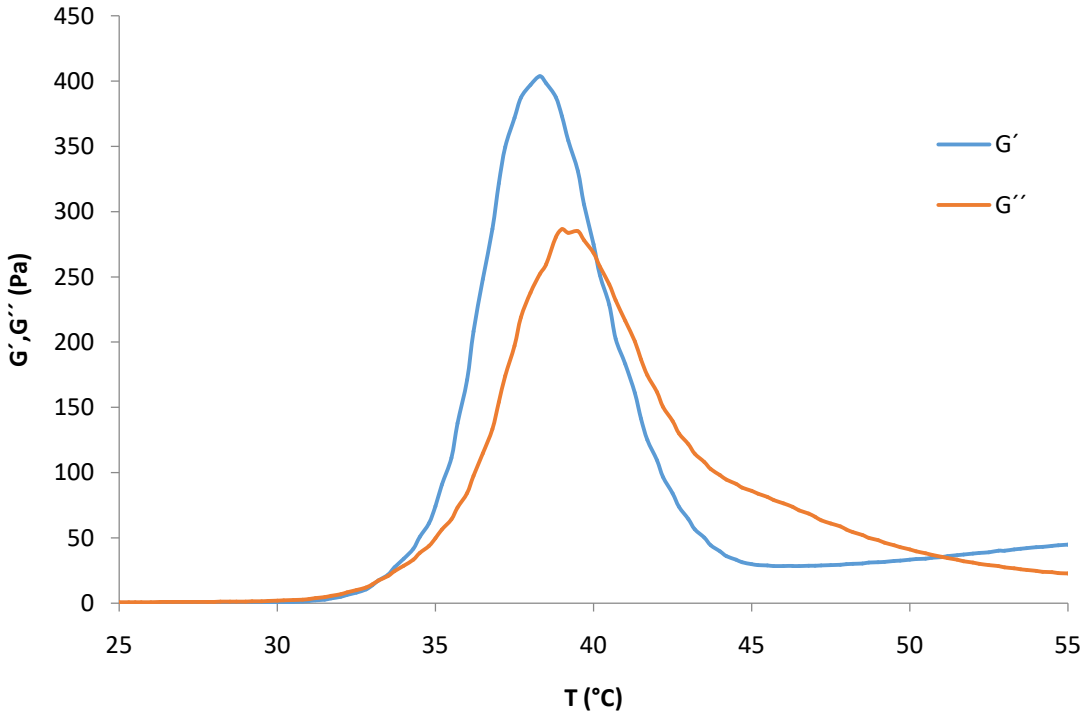

Figure 14: Rheology curves of PLGA-PEG-PLGA aqueous solution depicting visco-elastic properties.

5.1.2. α-tricalcium phosphate powder

The particle size distribution was obtained using laser scattering analyzer in ethanol suspension. Particles ranged from 3.905 to 7.697 μm in diameter with the most abundant fraction being 5.867 μm corresponding to 48.3 % of a total number of particles. Mean, median, mode size and standard deviation of particles were established. List of individual fractions and their distribution, as well as significant statistical data, are depicted in Table 5 and scattering plot is found in Figure 16 respectively.

Table 6: Abundance of individual fractions of α-TCP powder.

Number	Diameter [μm]	q [%]	Under Size [%]
44	3.905	0.191	0.191
45	4.472	3.249	3.440
46	5.122	22.607	26.047
47	5.867	48.347	74.395
48	6.720	23.708	98.100
49	7.697	1.900	100.000
Mean	**5.500**		
Median	**5.479**		
Mode	**5.490**		
Standard deviation	**0.614**		

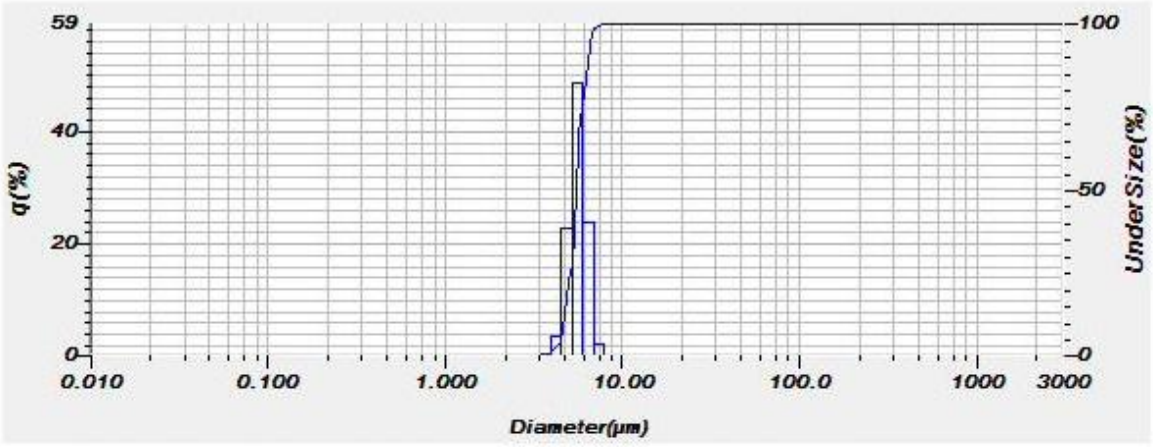

Figure 15: Laser scattering particle size distribution of α-TCP powder.

XRD analysis of α-TCP powder provided diffraction patterns which were evaluated and studied. Diffraction pattern in Figure 16 was established as a baseline for pure TCP. Changes in intensity of significant peaks during setting and hardening reactions were evaluated, and correspond to the transformation of TCP to CDHA. Significant diffraction peaks for pure monoclinic crystalline TCP are at 12.06, 14.02, 15.16, 22.20, 24.10, and 30.74 ° of 2θ [38]. FTIR analysis of powder showed dominant absorbance peaks at 1022 and 962 cm^{-1} wavenumbers. These peaks are interpreted according to Table 2. Region around 1022 cm^{-1} corresponds to anti-symmetric P-O triply degenerate stretching and peak at 962 cm^{-1} corresponds to symmetric P-O stretching [23]. FTIR spectrum is found in Figure 16. Illustrative example of α-TCP powder morphology is displayed on SEM image in Figure 18.

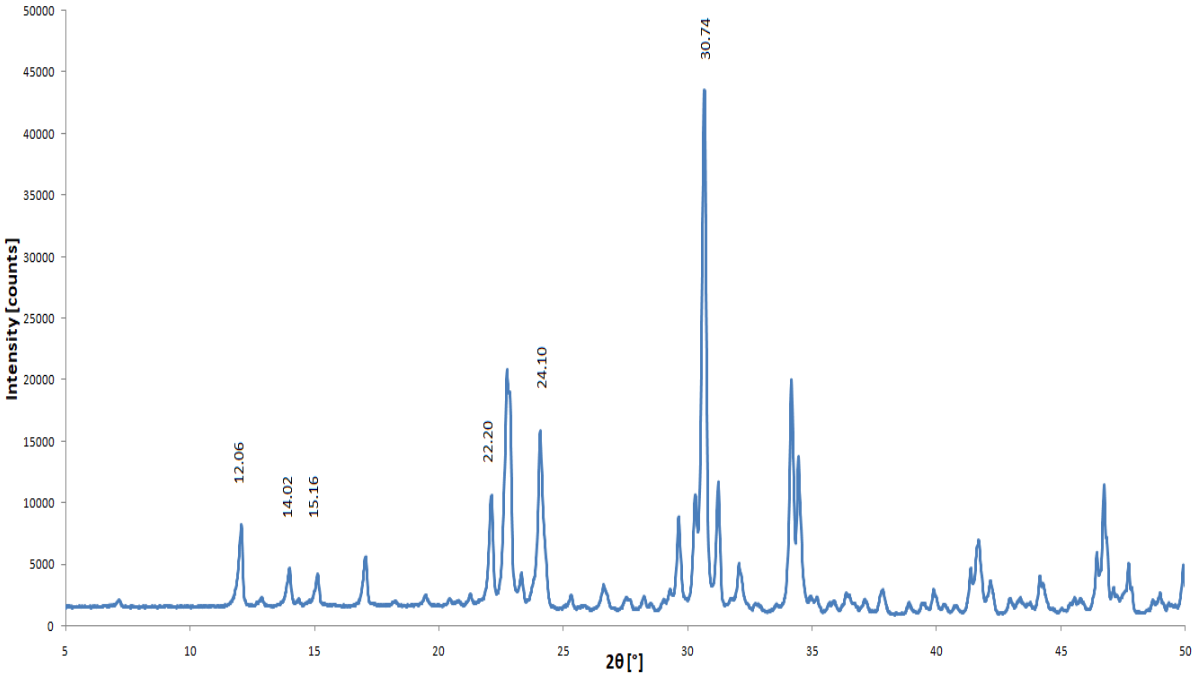

Figure 16: XRD diffractogram of pure, unreacted α-TCP powder.

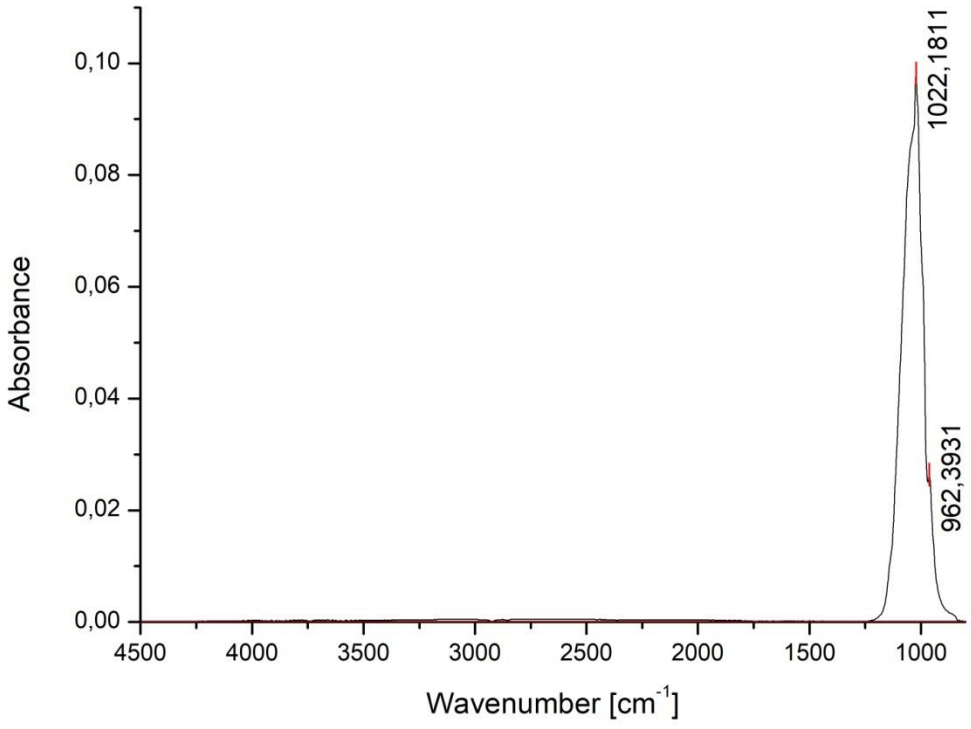

Figure 17: FTIR spectrum of pure, unreacted α-TCP powder.

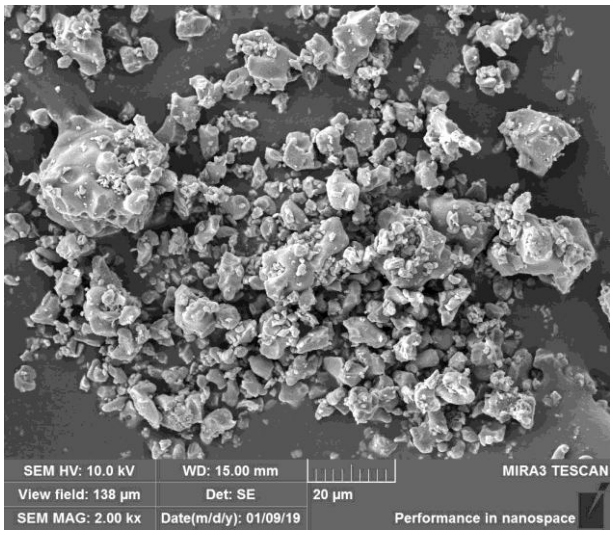

Figure 18: SEM image of pure, unreacted α-TCP powder.

5.1.3. PCL and PCL-Pluronic modified reinforcing fibers

Scanning electron microscope images of polymer fibers in Figure 19 showed that fibers exist in forms of bundles, not just the individual fibers. This is a result of electro spinning of the fibers, which produces a non-woven, randomly distributed fiber structure or bundle. Consecutive ultrasonic grinding and shredding of fibrous structure, provided cut fiber bundles with average size of 250 µm, which were used for the experiments. Diameter of individual fibers ranged from 2 to 10 µm.

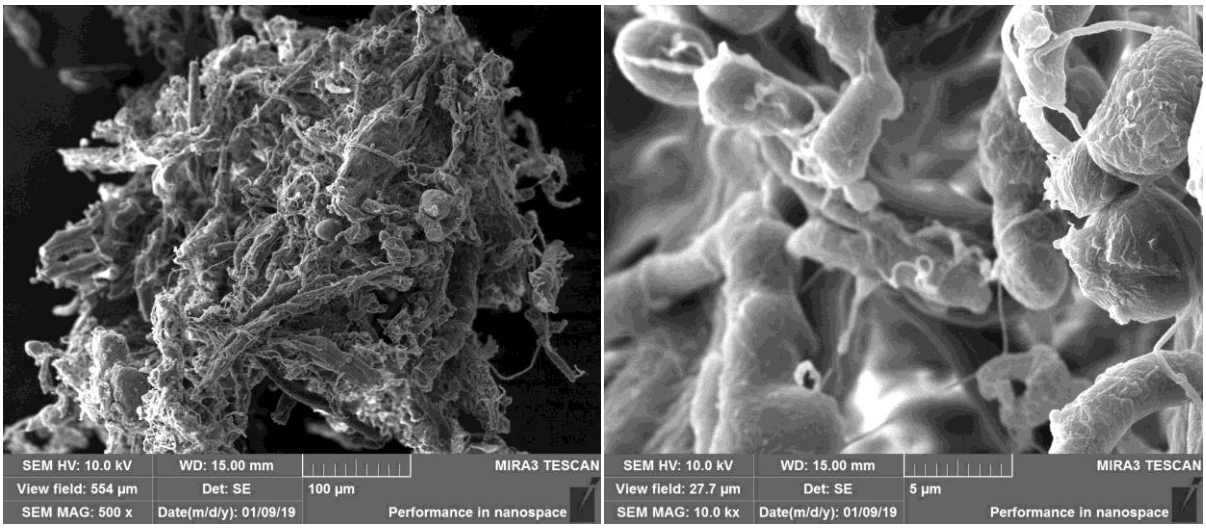

Figure 19: SEM images of polymer fibers.

FTIR analysis in Figure 20 and its spectral analysis provided information about fiber structure. The characteristic absorption bands at around 2942 and 2865 cm^{-1} are related to C-H stretching vibration of hydrocarbon of PCL. The band at 1724 cm^{-1} is ascribed to the stretching vibration of carbonyl groups (C=O) of PCL. The characteristic absorption bands in the fingerprint region of 958–1468 cm^{-1} are attributed to the deformation of $–CH_2–$ chain of PCL [59].

FTIR spectra of fibers overlapped with varying intensities, indicating that there are no observable structural differences between two types of fibers possibly due to low Pluronic content according to article [60].

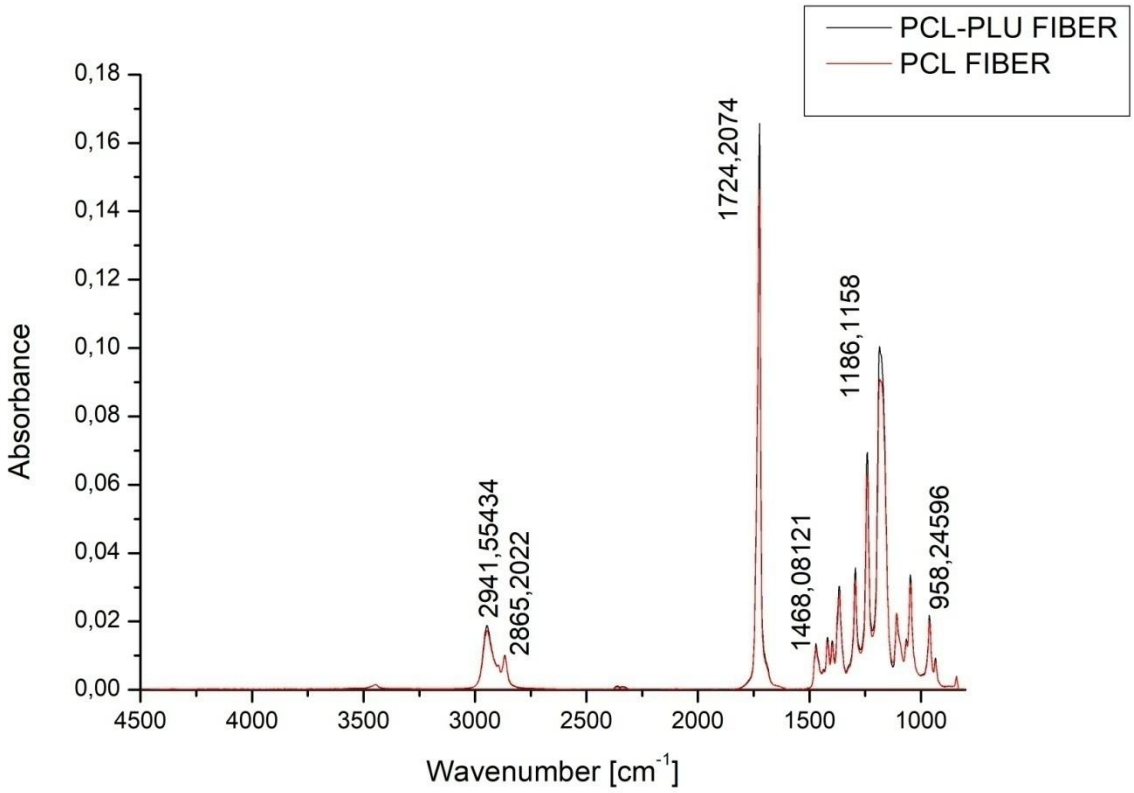

Figure 20: FTIR spectra of polymer reinforcing fibers.

5.2. Evaluation of rheological behavior and injectability

Rheological studies provided information about the setting of cement paste and injectability. Oscillatory time sweep measurement was used to establish materials transformation in time. As seen in Figures 21, 22 and 23 below, curves followed the same rising trend indicating setting and toughening of the paste which is to be expected due to the transformation of α-TCP to CDHA. Change in slope with addition of fiber reinforcements was observed. Setting of control paste was therefore faster than of the reinforced counterparts. The addition of polymer fibers increased the storage modulus (G') and consecutively stiffness of the paste. Significant differences between rheological performances of PCL-Pluronic and PCL reinforced pastes were not observed.

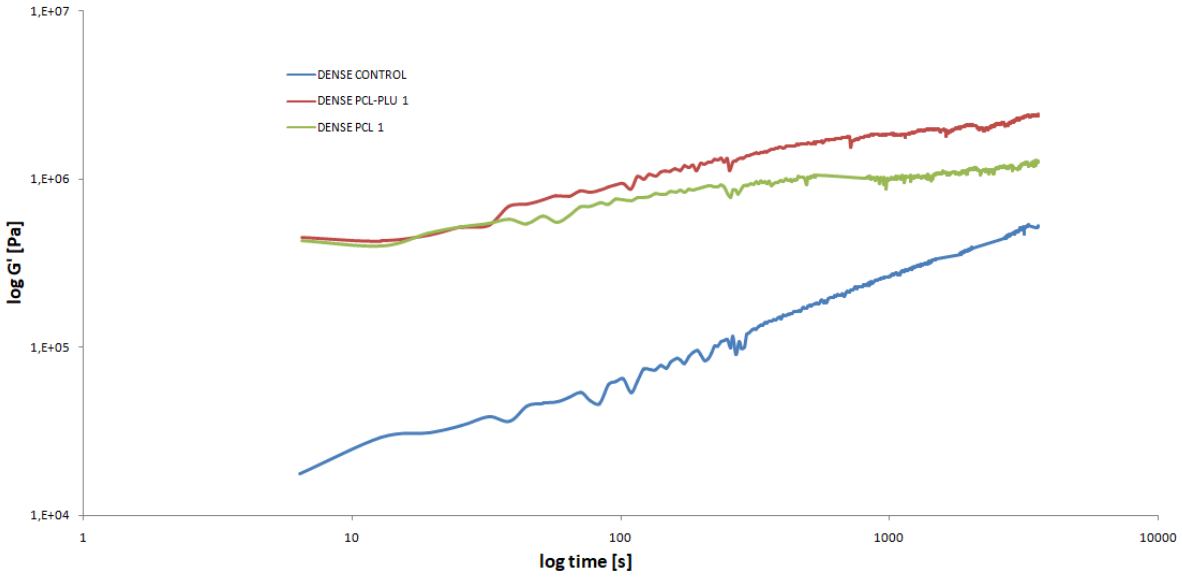

Figure 21: Time sweep rheological curves of dense samples at 23 °C.

With the addition of more fibers, even higher increase in storage modulus was observed for both types of fibers. Lower values of initial storage modulus were obtained for PCL-PLU reinforced samples compared to PCL reinforced ones. Differences are within the margin of error, which could be caused by more thorough mixing of the paste during preparation.

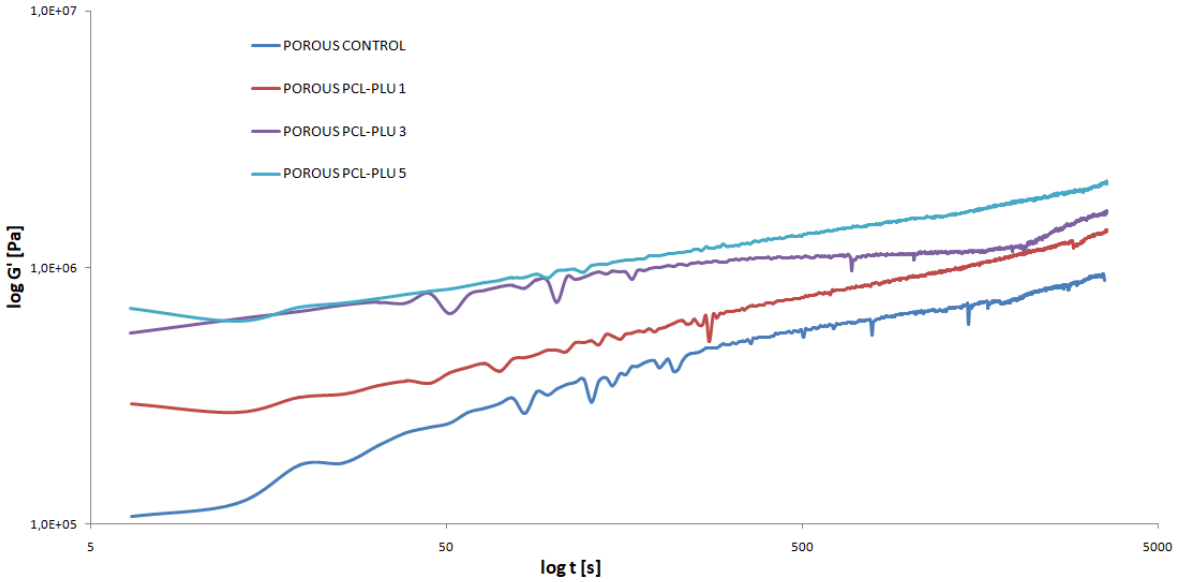

Figure 22: Time sweep rheological curves of PCL-Pluronic reinforced porous samples at 23 °C.

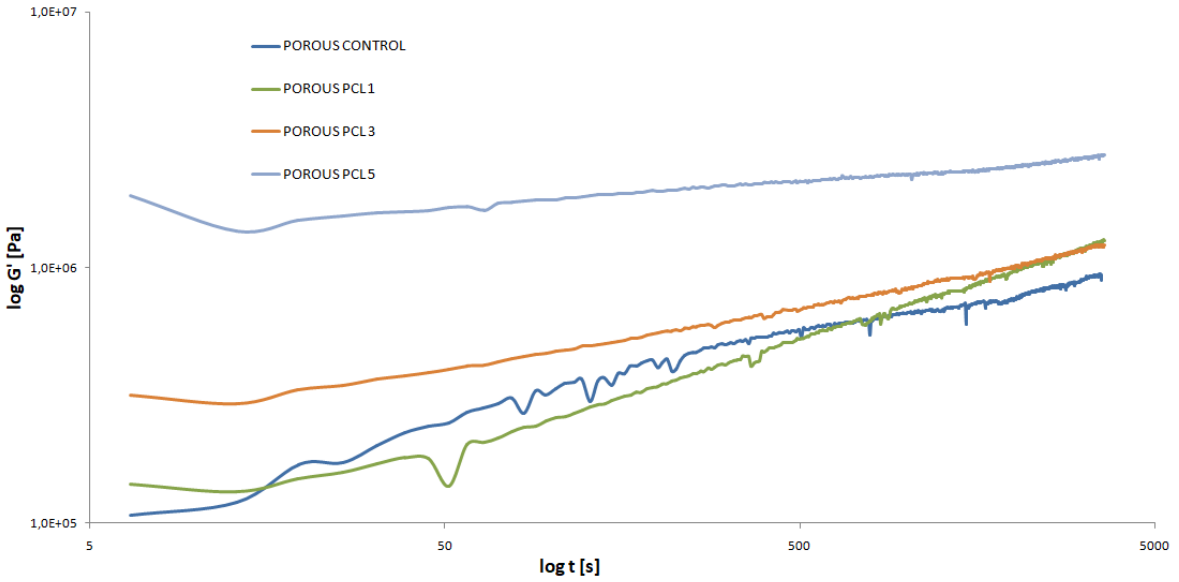

Figure 23: Time sweep rheological curves of PCL reinforced porous samples at 23 °C.

Higher fiber additives e.g. 5 wt. %, started with even larger initial values of storage modulus. 5 weight percent addition of both types of fibers proved too difficult to inject via syringe. Fibers prevented the flow of the paste i.e. increased the storage modulus and stiffness, the fact is supported by the image in Figure 24. Therefore, 5 wt. % fiber additives were deemed unsuitable for use in surgical practice and focus was targeted more on lower fiber contents.

Figure 24: Failure of injectability for samples with 5 wt. % fiber additive.

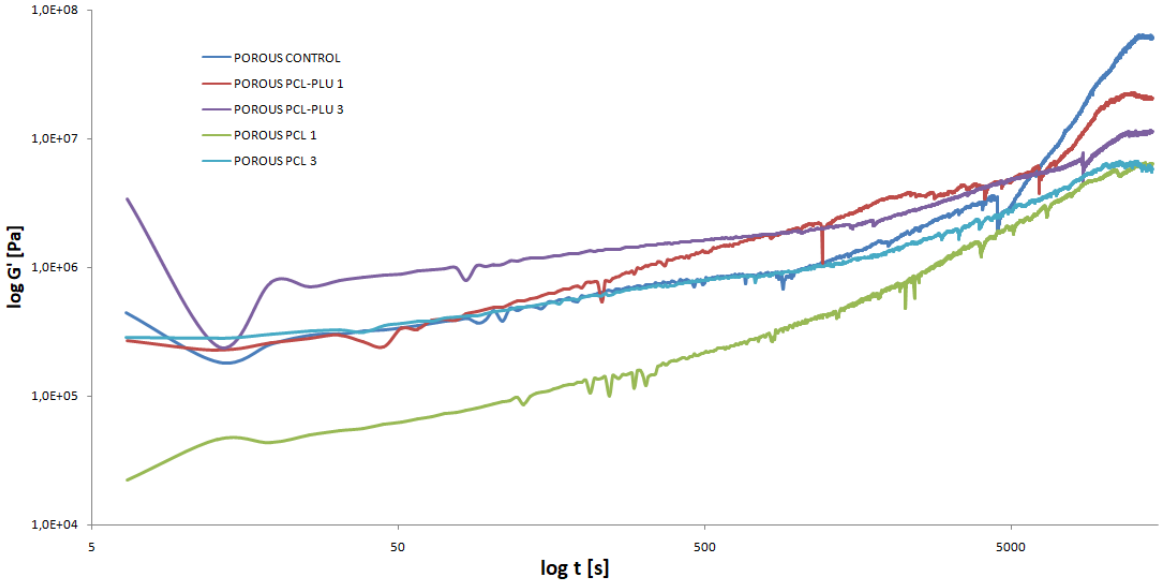

Figure 25: Time sweep rheological curves of reinforced porous samples at 37 °C.

Rheological studies at 37 °C showed similar trends. Maximum storage modulus was reached at around 3 hours and 30 minutes mark for all the tested samples with minor deviations within margin of error. This means, that fibers did not greatly interfere with paste setting. The decrease in storage modulus of reinforced samples at 37 °C is explained precisely by the addition of fibers which are softer than the ceramic matrix. Setting reaction transforms α-TCP to CDHA; this solidifies the paste and is the dominant component responsible for final toughness. Addition of fibers, therefore, produces composite which in turn has lower storage modulus.

5.3. Mechanical properties testing

Mechanical testing was performed on INSTRON 8874 testing machine. Compression strength (CS) tests were conducted on dry cylindrical samples with 6 mm in diameter and 9 mm of height. The compression rate was set up to 1 mm/min. CS values were calculated as the maximum stress a sample could withstand before fracture, divided by sample surface area in millimeters squared. Elastic moduli (E) were evaluated from stress-strain curves. Stress-strain curve contained linear onset. This region contained the most linear gains, therefore was used to establish Young's elastic modulus using the linear regression method. The values containing average values and standard deviations of CS and E for each set of dense and porous samples are found in Tables 7 and 8. Representative stress-strain curves of dense and porous samples, as well as the comparison of CS and E with corresponding error bars, are displayed in Figures 26, 27, 28, 29, 30 and 31.

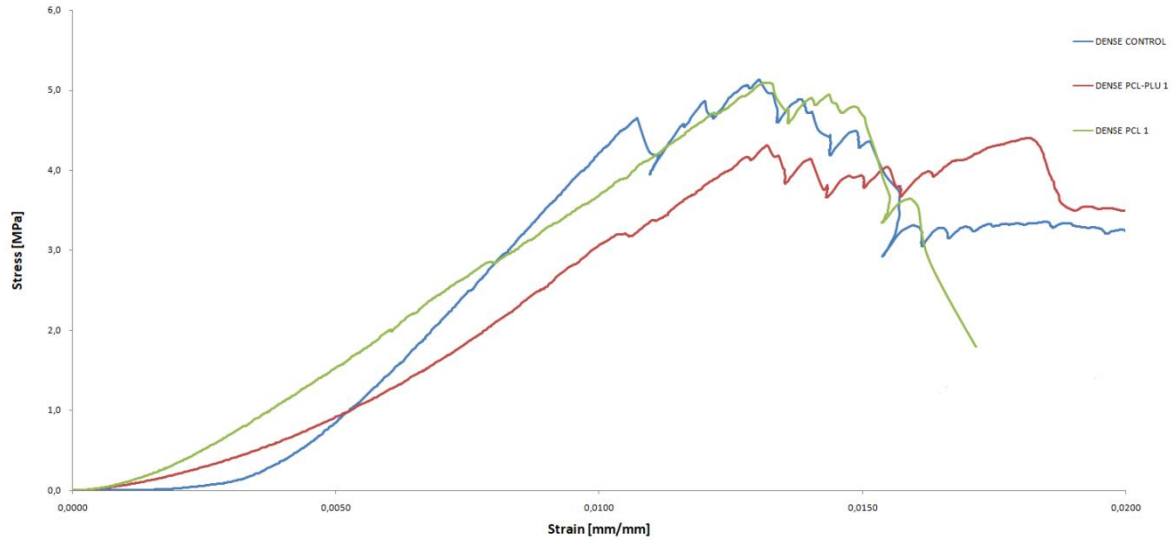

Figure 26: Representative stress-strain curves of dense samples.

As seen in Figure 26, deformation of material starts with a transient non-linear stage explained by insufficient flatness of contact surfaces. Curve then follows a linear slope until deformation reaches a critical value of proportional limit, rapidly exceeding maximum withstandable stress resulting in a catastrophic fracture. The jagged curve before maximum load, obtained for dense control sample, can be explained by cracking of material near defects or pores present in the material's structure.

Table 7: Summary of average compressive strengths, elastic moduli, and their standard deviations of dense samples.

Sample	Average CS [MPa]	St. Dev CS [MPa]	Average E [GPa]	St. Dev E [GPa]
DENSE CONTROL	5.23	± 0.58	0.54	± 0.19
DENSE PCL-PLU wt. 1 %	4.87	± 0.98	0.38	± 0.15
DENSE PCL wt. 1 %	4.96	± 0.35	0.42	± 0.14

The addition of 1 wt. % of both types of polymer fibers resulted in a slight decrease in the average compressive strength of samples. Statistical analysis of samples did not confirm significant differences in results. Fibers tended to clump together during sample preparation. Therefore, the mixing of cement paste with spatula seemed to be an inefficient way of homogenizing them in a ceramic matrix, resulting in possibly lower compressive strengths.

Ceramics in general, are brittle materials. This especially applies to bone cements. Samples possess low values of elastic modulus due to their intrinsic porosity. Interestingly yet, a decrease of elastic modulus values of dense samples signifies some degree of fiber reinforcing capabilities. High scattering of values resulting in large standard deviations, might be explained by inhomogeneous distribution of pores. T-test analysis did not prove any statistically significant differences due to large scattering of obtained values. Moduli are therefore considered as an indicative values.

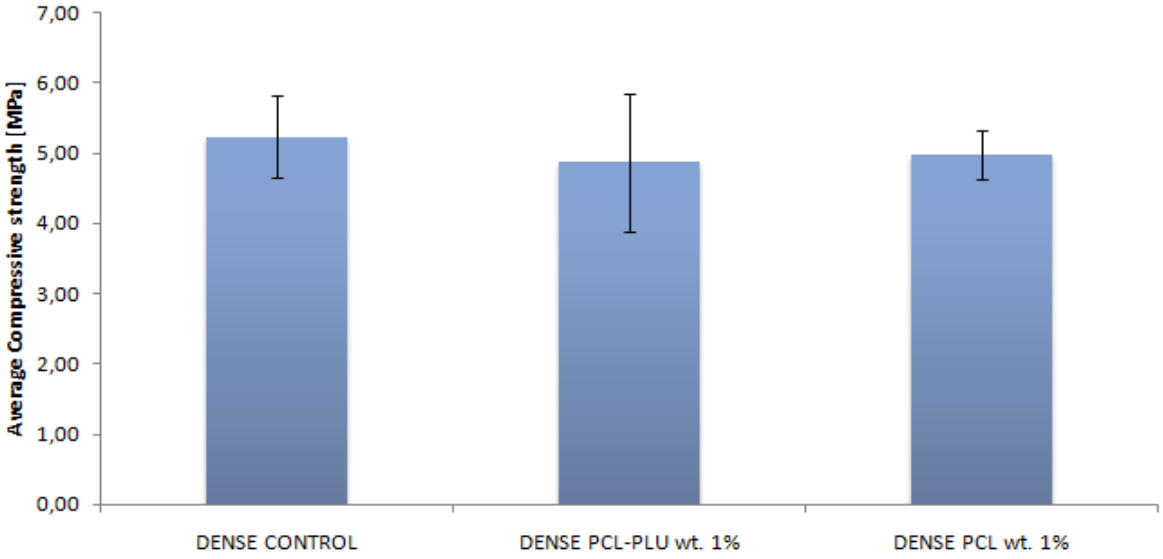

Figure 27: Graphical representation of average compressive strengths of dense samples.

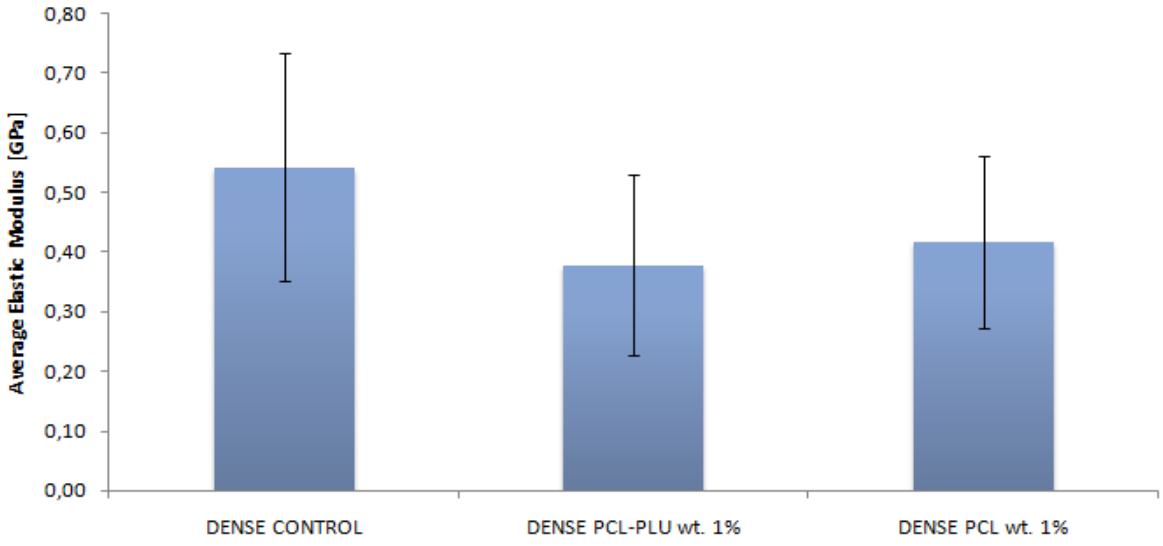

Figure 28: Graphical representation of average elastic moduli of dense samples.

Due to higher potential inhomogeneity of fibers in dense samples, the focus of the thesis was directed more on porous samples mixed with XENOX Roti speed-stirring mixer. The assumption of better osteointegration and cell growth on the material's surface with increasing sample porosity was also one of the factors of an emphasis on porous samples in this thesis.

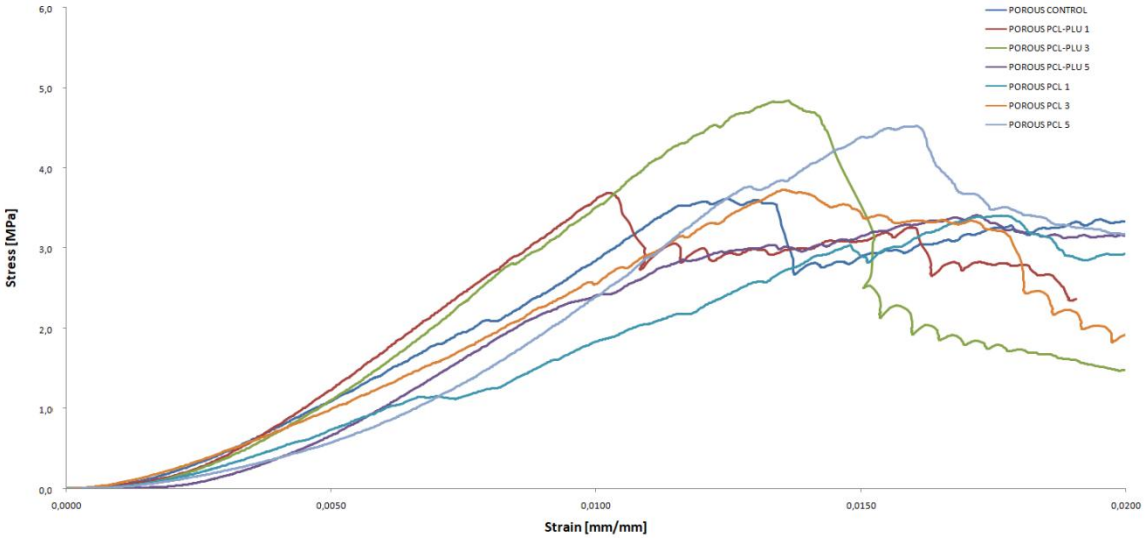

Figure 29: Representative stress-strain curves of tested porous samples.

The same conclusions about curve shapes can be applied for porous samples as well. Transient non-linear initial stage, linear slope and ultimate strength before fracture can be observed from curves in Figure 29.

Table 8: Summary of average compressive strengths, elastic moduli, and their standard deviations of porous samples.

Sample	Average CS [MPa]	St. Dev CS [MPa]	Average E [GPa]	St. Dev E [GPa]
POROUS CONTROL	3.31	± 0.17	0.43	± 0.14
POROUS PCL-PLU wt. 1 %	3.69	± 0.67	0.43	± 0.24
POROUS PCL-PLU wt. 3 %	4.77	± 0.79	0.45	± 0.14
POROUS PCL-PLU wt. 5 %	3.77	± 0.38	0.40	± 0.07
POROUS PCL wt. 1 %	3.54	± 0.76	0.39	± 0.17
POROUS PCL wt. 3 %	3.90	± 0.65	0.45	± 0.12
POROUS PCL wt. 5 %	4.44	± 0.50	0.44	± 0.13

With the addition of polymer fiber reinforcements, a slight increase in ultimate strength of the material is observed. The maximum increase in compressive strength for porous samples was observed for samples with 3 wt. % of PCL-Pluronic reinforced and 5 wt. % of PCL fiber reinforced samples respectively. Statistical analysis of obtained values proved significant difference for mentioned samples. Increasing the fiber content in the ceramic matrix follows a

rising trend. Deviation from this trend is found in sample reinforced with 5 wt. % PCL-Pluronic fibers. This anomaly might be explained by large quantity of fibers, and their insufficient homogeneity in the ceramic matrix. Inhomogeneity has been detected with SEM analysis. Nonetheless, all of the reinforced sample values possess quite a large compressive strength standard deviation. This might be the contribution surface flaws and of pores introduced by thorough mixing which are not uniform, and their distribution influences maximum compressive strength.

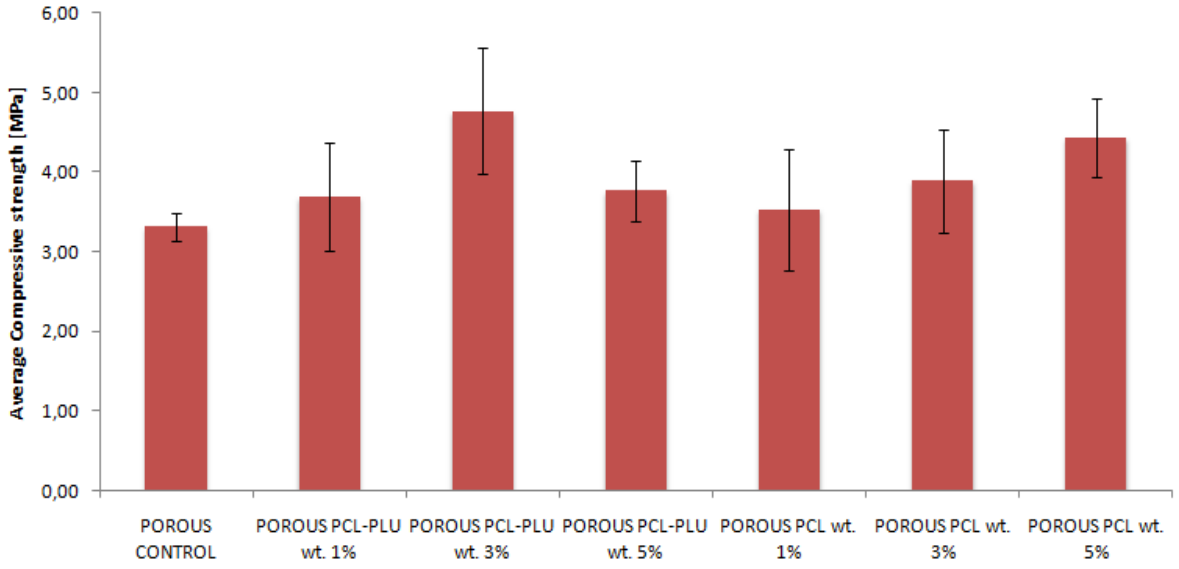

Figure 30: Graphical representation of average compressive strengths of porous samples.

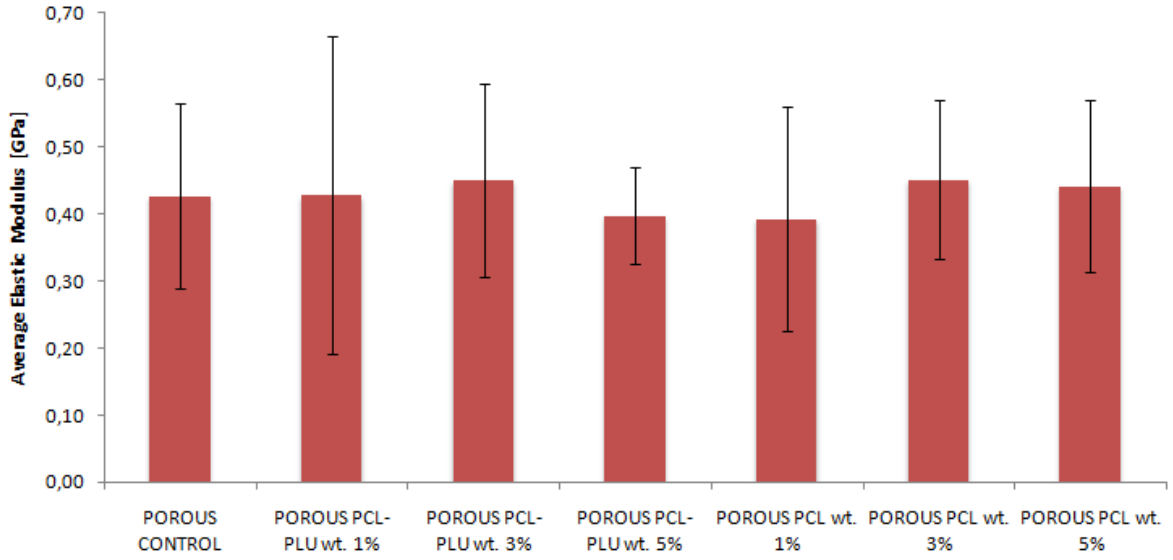

Figure 31: Graphical representation of average elastic moduli of porous samples.

Comparison between modified PCL-PLU and PCL fiber additives shows a slight increase in compressive strengths as well. Namely, the 3 wt. % fiber additive shows a significant increase, supported by T-test statistical analysis. This can be attributed to the amphiphilic nature of modified PCL-Pluronic fibers, resulting in possibly better fiber into matrix incorporation compared to hydrophobic PCL fibers.

According to Panzavolta et al. in article [32] values of elastic moduli are expected to decrease with the addition of polymer reinforcements, rendering material more ductile. Present macropores introduced via speed-stirring mixing reduce the elastic modulus values as well. Observed E is, therefore, quite low. However, decrease in elastic modulus with a higher fiber content of porous samples in this thesis was not overwhelmingly observed. Due to the large scattering of values, statistics proved no significant differences in elastic moduli values. However, again, standard deviations for elastic moduli are quite high, therefore elastic modulus values are considered just as an apparent or indicative value.

To establish tensile strengths of the most promising samples, disc samples with a diameter of 10 mm and a height of 4 mm were prepared and tested using so-called Brazilian test or diametrical tensile strength test. The Brazilian test is a simple indirect testing method to obtain the tensile strength of brittle materials. The compression induces tensile stresses normal to the vertical diameter, which are essentially constant over a region around the center. The indirect tensile strength is therefore calculated based on the assumption that failure occurs at the point of the highest tensile strength i.e. at the center of the sample. The suggested formula for diametrical tensile strength (DTS) is displayed in the equation 9 below, where F is maximum applied load before crack, d is the diameter of disc sample and h is the thickness of the sample. Stress-strain curves were produced using diametric strain – the ratio between crosshead displacements and sample diameter, and diametric stress.

$$\sigma_t(\mathrm{DTS}) = \frac{2 \cdot F}{\pi \cdot d \cdot h} \tag{9}$$

The tests were conducted in a dry state and wet state to simulate the performance of the material at physiological conditions. Dry samples were removed from the incubator after 10 days and dried in a desiccator, whereas wet samples were kept in distilled water tempered to 37 °C until the mechanical tests.

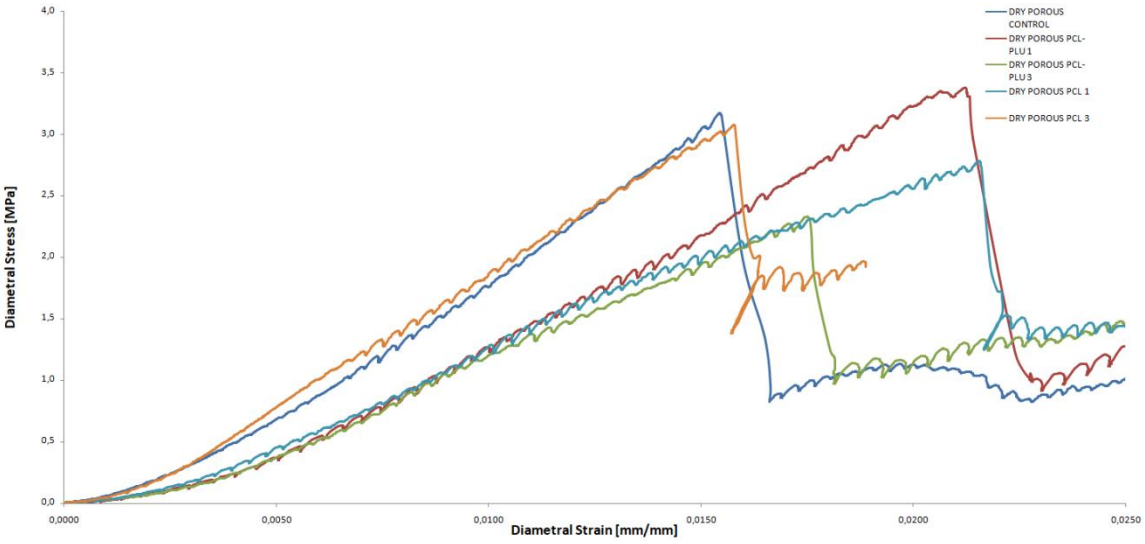

Figure 32: Representative diametrical stress-strain curves of tested dry porous samples.

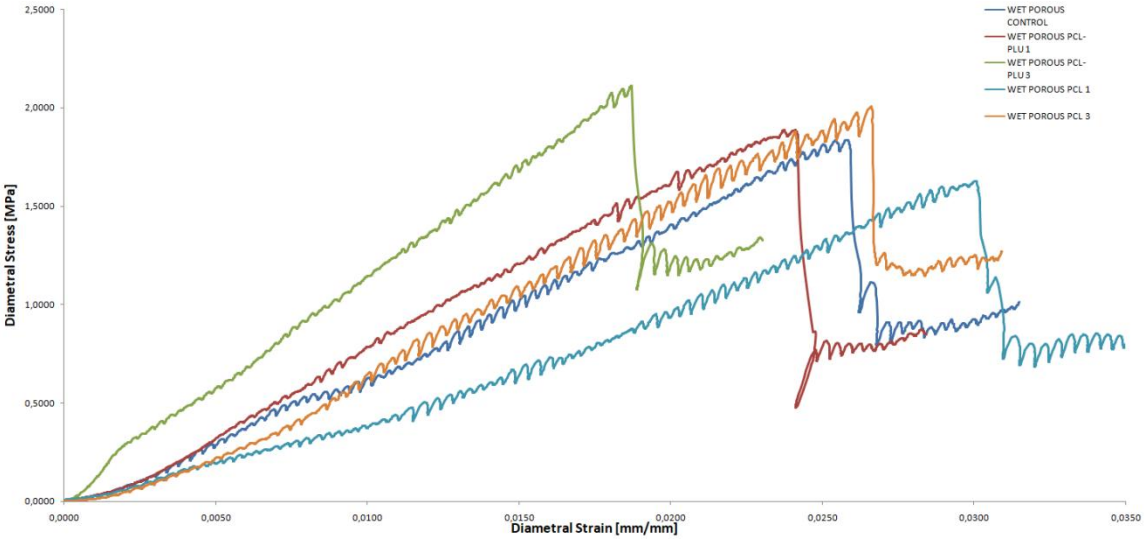

Figure 33: Representative diametrical stress-strain curves of tested wet porous samples.

As seen in Figures 32 and 33, after the maximum stress was reached, crack passing through the entire testing body occurred. Control samples seemed to have just one interconnected crack, propagating from either top or top and bottom part of sample, splitting sample into two pieces, while reinforced samples showed one main crack with branching. Small changes in linear slopes have been observed, indicating certain low degree of reinforcing capabilities.

Figure 34: Observance of cracks for porous control sample (left), PCL-PLU 1 wt. % reinforced samples (two in the middle) and PCL-PLU 3 wt. % (right).

Table 9: Summary of average diametrical tensile strengths and their standard deviations of dry and wet porous samples.

Sample	DRY		WET	
	Average DTS [MPa]	St. Dev DTS [MPa]	Average DTS [MPa]	St. Dev DTS [MPa]
POROUS CONTROL	3.18	± 0.50	1.82	± 0.19
POROUS PCL-PLU wt. 1 %	3.33	± 0.60	1.91	± 0.25
POROUS PCL-PLU wt. 3 %	2.28	± 0.22	1.87	± 0.44
POROUS PCL wt. 1 %	2.80	± 0.63	1.66	± 0.26
POROUS PCL wt. 3%	3.08	± 0.49	1.91	± 0.21

Nonetheless, a statistically significant decrease in diametrical tensile strength has been observed for 3 wt. % PCL-Pluronic reinforced samples. Performance of samples in compressive and tensile domain differ as well. This applies especially for samples reinforced with 3 wt. % PCL-PLU fibers. The phenomenon might be explained by the different nature of tests. Compression induces force which closes pores. Fibers possess some elasticity and deform under load, which in turn increases compressive strength due to better distribution of stresses in the material. Diametrical tensile strength tests open the pores, some of which can be filled with polymer fibers. Used polymer fibers seemed to have low tensile strength, diminishing the tensile strength of the material. Nonetheless, compressive strength is more important parameter for bone cement applications.

From obtained values, it is possible to state that samples kept in distilled water at physiological conditions performed worse compared to dry porous samples, the decrease is most obvious from Figure 35. Water possibly softens ceramic matrix causing it to become more brittle, resulting in fracture at lower stresses. Statistical analysis did not prove any significant changes in DTS values for wet samples. Addition of fiber reinforcements, therefore, did not have an observable effect on samples performance in diametrical tensile strength domain.

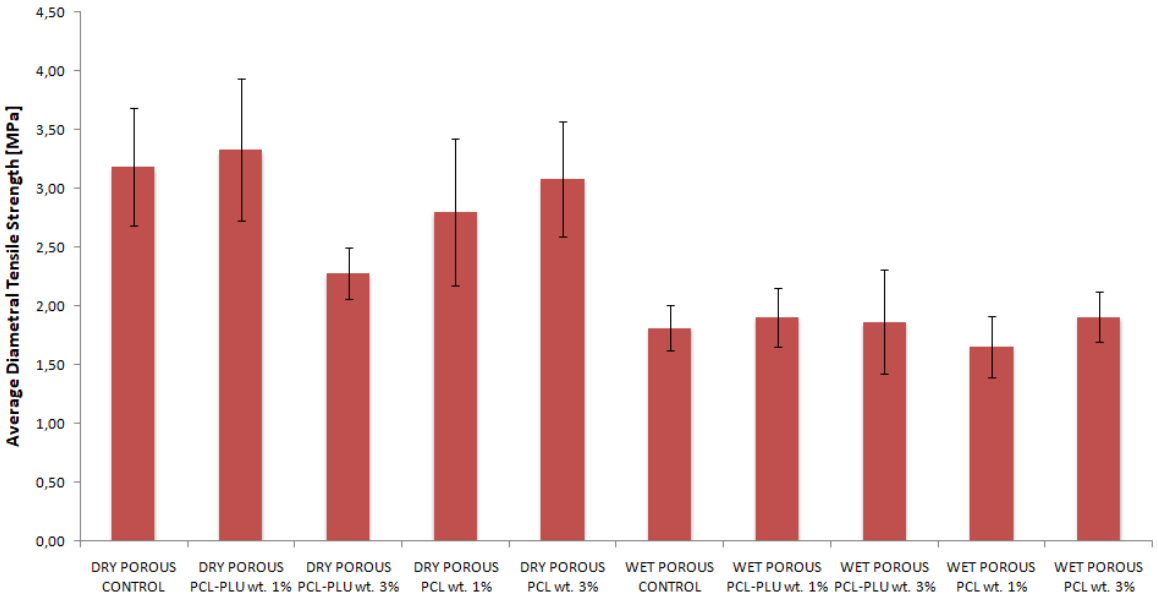

Figure 35: Graphical representation of average diametrical tensile strengths of porous samples.

5.4. Microstructure analysis

Microstructure and fiber integration were observed using the TESCAN MIRA3 XMU scanning electron microscope. Observance of microstructure proved transformation of α-TCP to CDHA as expected. No unreacted grains of α-TCP powder remained, therefore was concluded, that α-TCP underwent total or almost total transformation to CDHA after 10 days of setting at 37 °C in incubator. The emergence of well developed needle-like and plate-like CDHA crystals was detected. Needle-like crystals were attributed to rapid hydrolysis of fine α-TCP particles. Plate-like particles started crystallizing from coarser particles of α-TCP powder [38]. Mixing had apparently also a slight influence on crystal morphology. Samples hand-mixed with spatula contained more plate-like crystals as seen on the left side in Figure 36 below compared to image of speed-stirred samples on right.

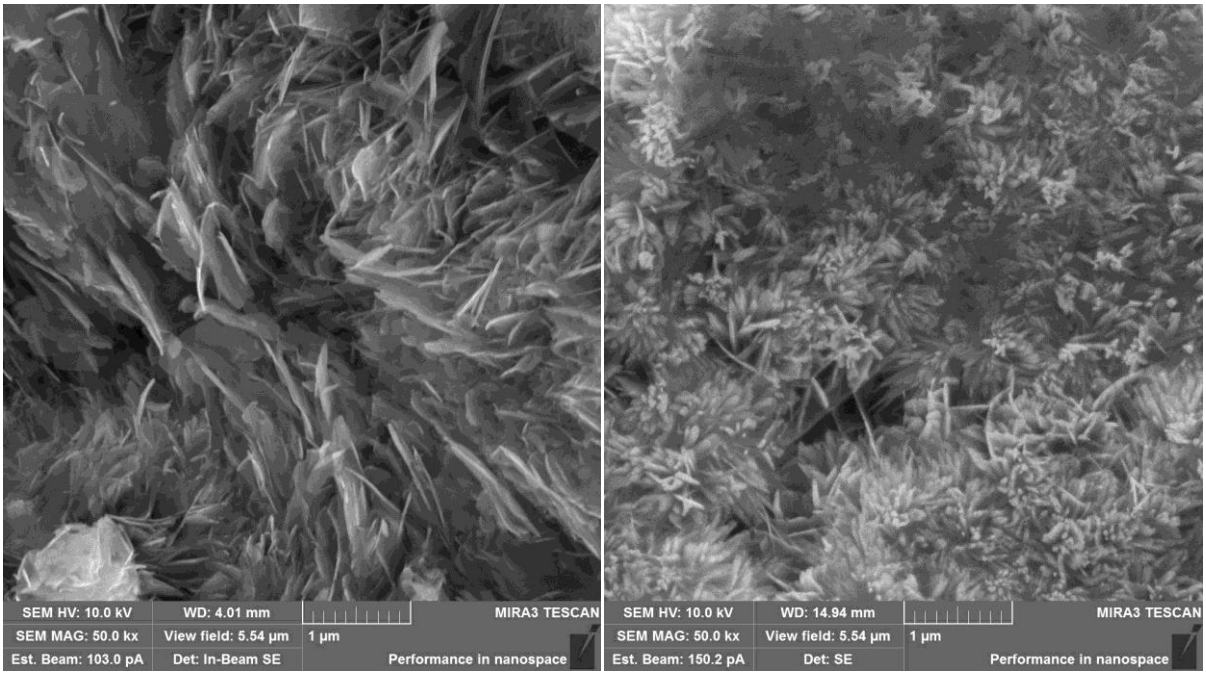

Figure 36: Microstructure of dense (left) and porous (right) sample.

Presence and identification of fiber reinforcements was most notable using detector for back-scattered electrons. Due to their structure, fibers are mainly made up from carbon and oxygen polymer chains while ceramic matrix contains calcium and phosphorus atoms. Ca and P have much higher atomic weight than C and O. Therefore, back-scattered electrons are deflected by atomic nuclei much more. This produces contrast, increasing detection intensity, and proved to be better identification technique for fiber reinforcements. In the Figure 37, it is possible to observe this phenomenon with comparison to secondary electron and back-scattered electron detectors. Fibers in Figure 37 are therefore of darker color while ceramic matrix is much lighter in color.

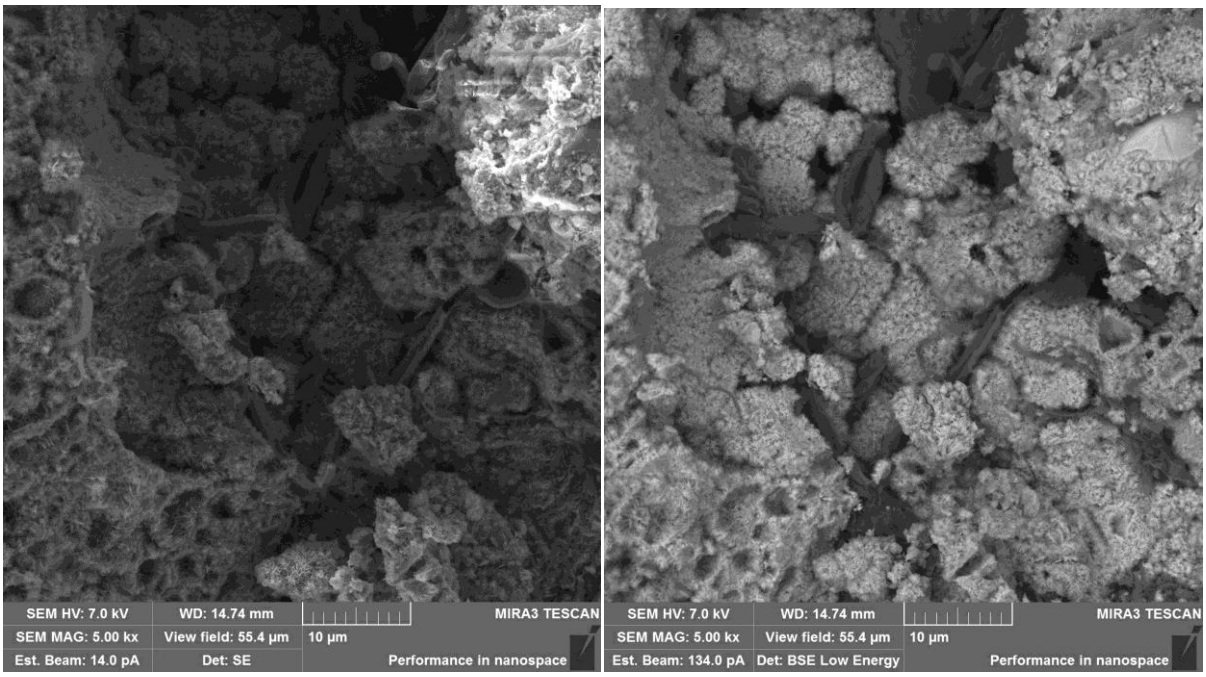

Figure 37: SEM images of same spot with secondary electron (left) and back-scattered electron detectors (right). Fibers are dark fibrous structures; ceramic matrix is displayed as light spiky grains.

Integration of polymer fibers into ceramic matrix was investigated. Crack interfaces of 3 wt. % reinforced samples used for DTS tests were studied under SEM. Fiber reinforced composite failure modes were studied, nonetheless, very low degree of fiber fractures and fiber pull-outs were detected. Only small amount of CDHA crystals seem to adhere to the present fibers resulting in poor fiber-ceramic matrix adhesion. This might cause poor stress transfer during mechanical testing, diminishing/not improving mechanical properties. Therefore, it was concluded that fiber reinforcing capabilities are quite low.

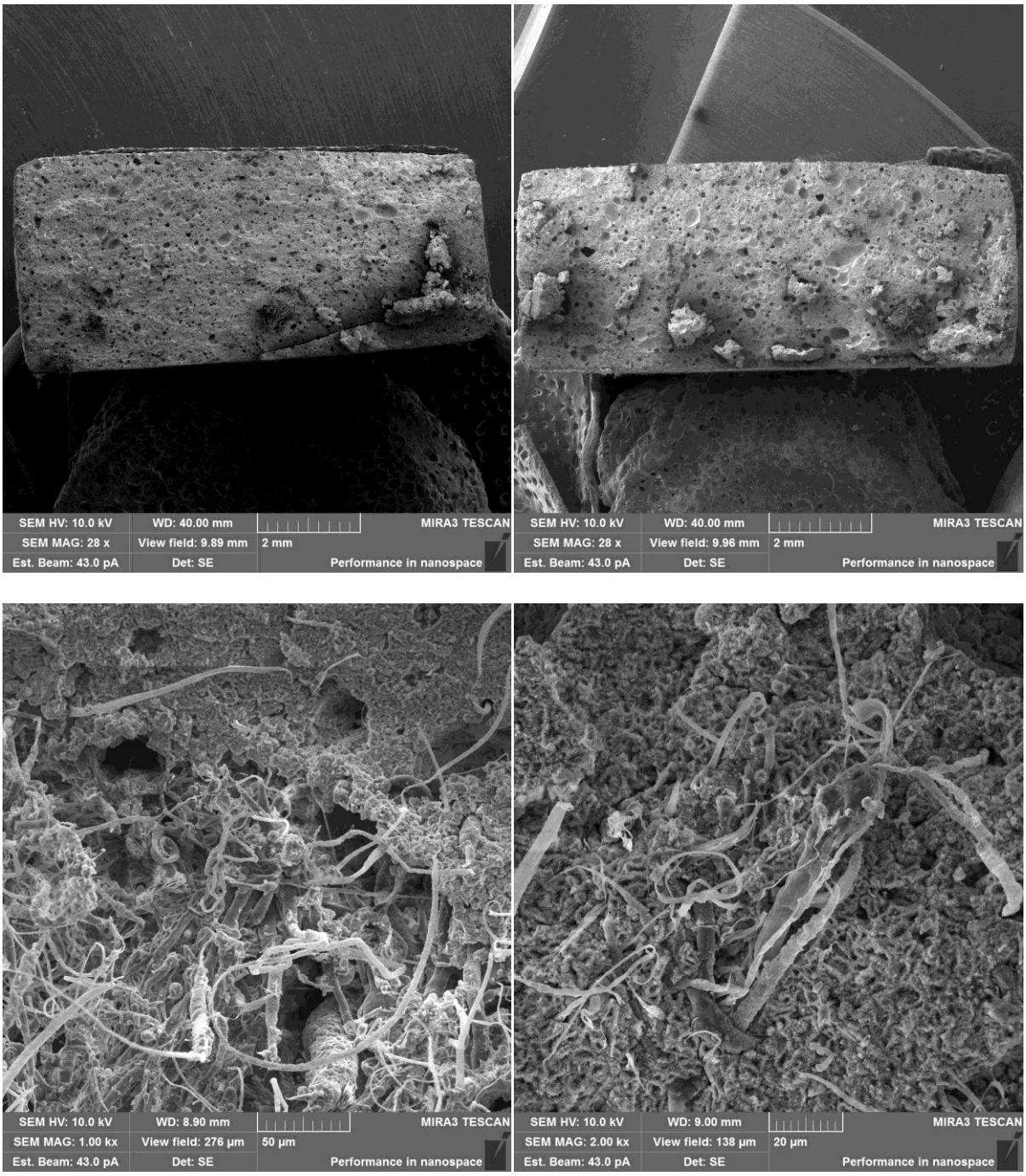

Figure 38: SEM images of DTS samples, 3 wt. % PCL (left) and PCL-PLU (right) reinforced samples.

Potential fiber inhomogeneity has been detected using SEM imaging in Figure 39. Clumping of fibers during sample preparation and insufficient homogenization resulted in bundles of fibers inside ceramic matrix. Fiber inhomogeneity in cement paste during sample preparation could contribute to uneven fiber distribution from sample to sample. This fact contributes to the high scattering of obtained values of mechanical properties.

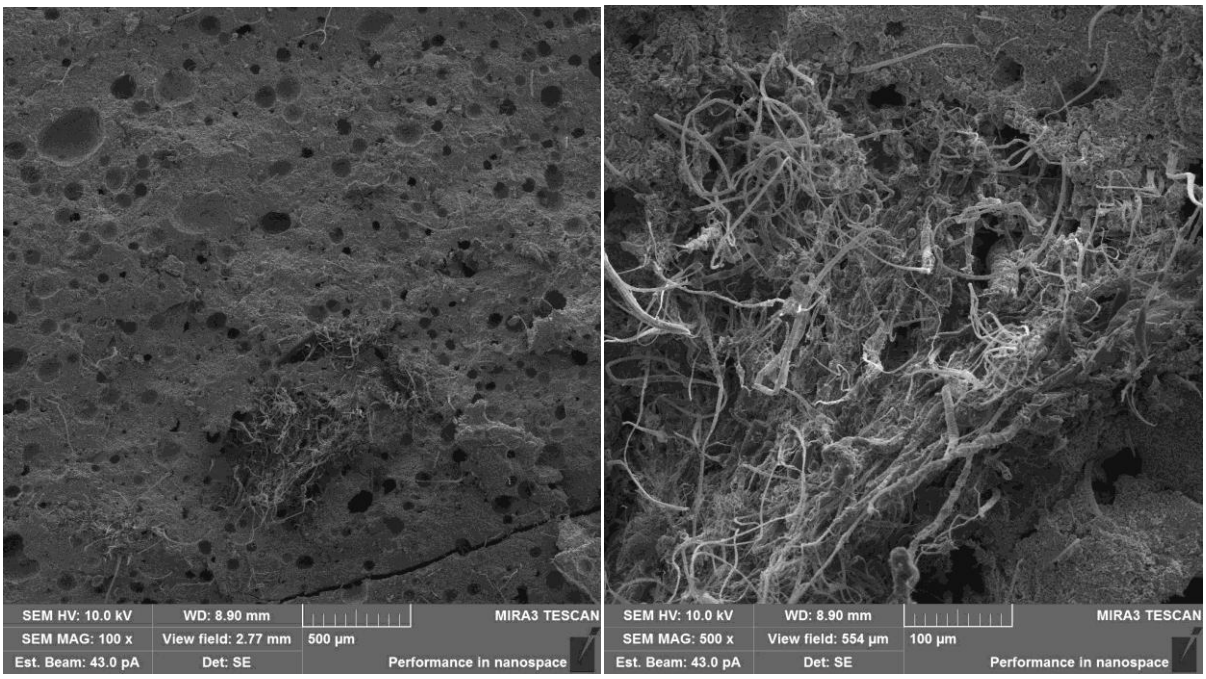

Figure 39: SEM images of present fiber inhomogeneity.

5.5. Determination of porosity

Porosity was measured using micro-computer tomography (micro-CT). Due to advanced nature of method and device's high operation cost, only 4 samples were analyzed, A – Dense control sample, B – Porous control sample, C – Dense 1 wt. % PCL-PLU reinforced sample and D – Porous 1 wt. % PCL-PLU reinforced sample. Pore distribution from micro-CT analysis and images of samples themselves are displayed in Figures 40 and 41.

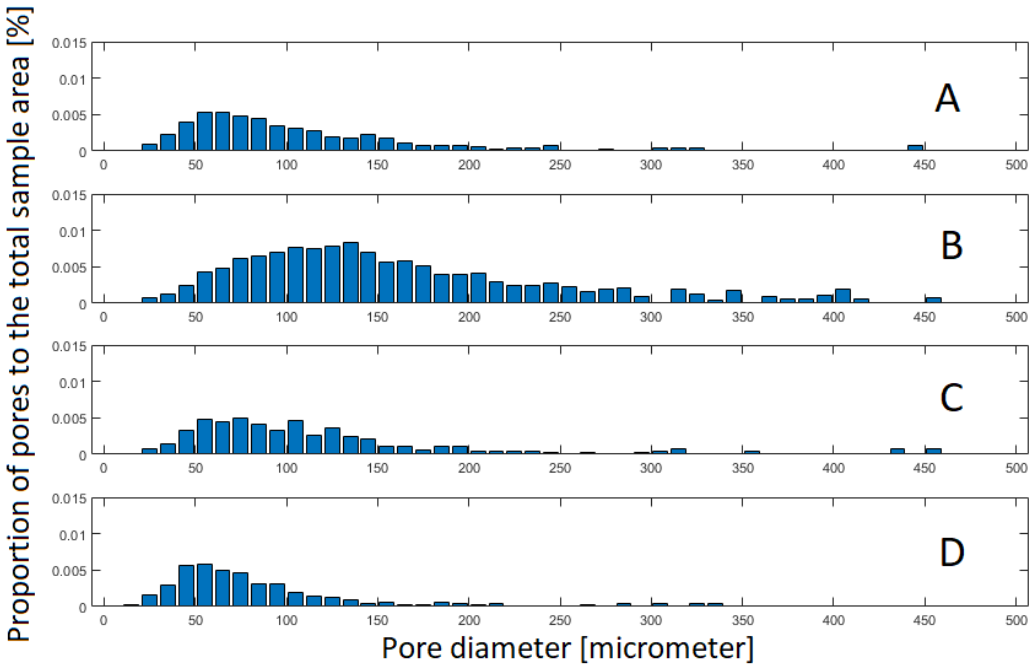

Figure 40: Pore distribution of tested samples A: Dense control sample, B: Porous control sample, C: Dense 1 wt. % PCL-PLU fibers reinforced sample, D: Porous 1 wt. % PCL-PLU fibers reinforced sample.

As seen in the Figure 40 above, the mixing of control sample with speed-stirring mixer did indeed increase the porosity of the sample compared to spatula mixing. Porous sample pore size compared to dense sample also increased; distribution of pores changed and larger pores emerged. This finds its applications in osteoconductivity but unfortunately, higher porosity had a negative effect on mechanical properties as seen from mechanical tests. Addition of polymer fibers did not have a significant influence on dense samples porosity. However, polymer fibers are biodegradable and after they undergo degradation, pores are left in their place. Fiber addition to speed-stirred sample somehow hindered porosity observed via micro-CT. Tangled bundles of fibers seem to close pores during the mixing; nonetheless, fibers should still increase the porosity of material after they are degraded away. For illustrative purposes cross sections of tested samples are displayed in Figure 42.

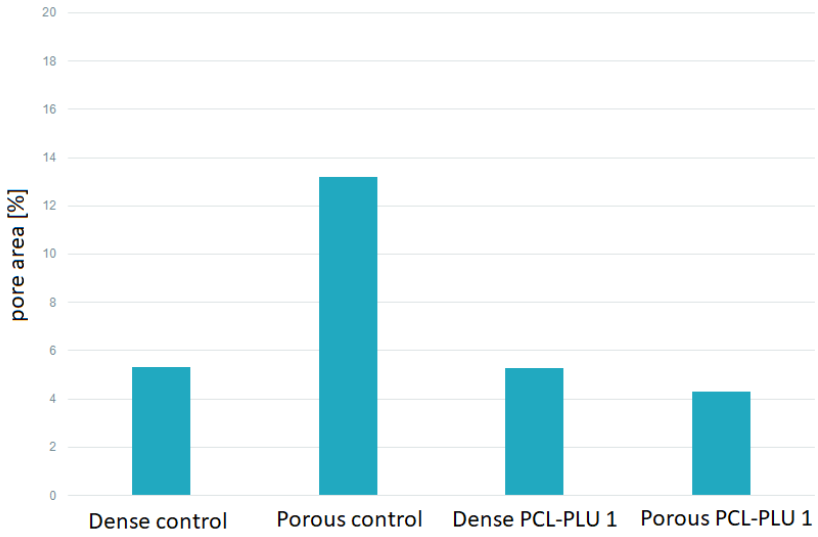

Figure 41: Porosity of tested samples.

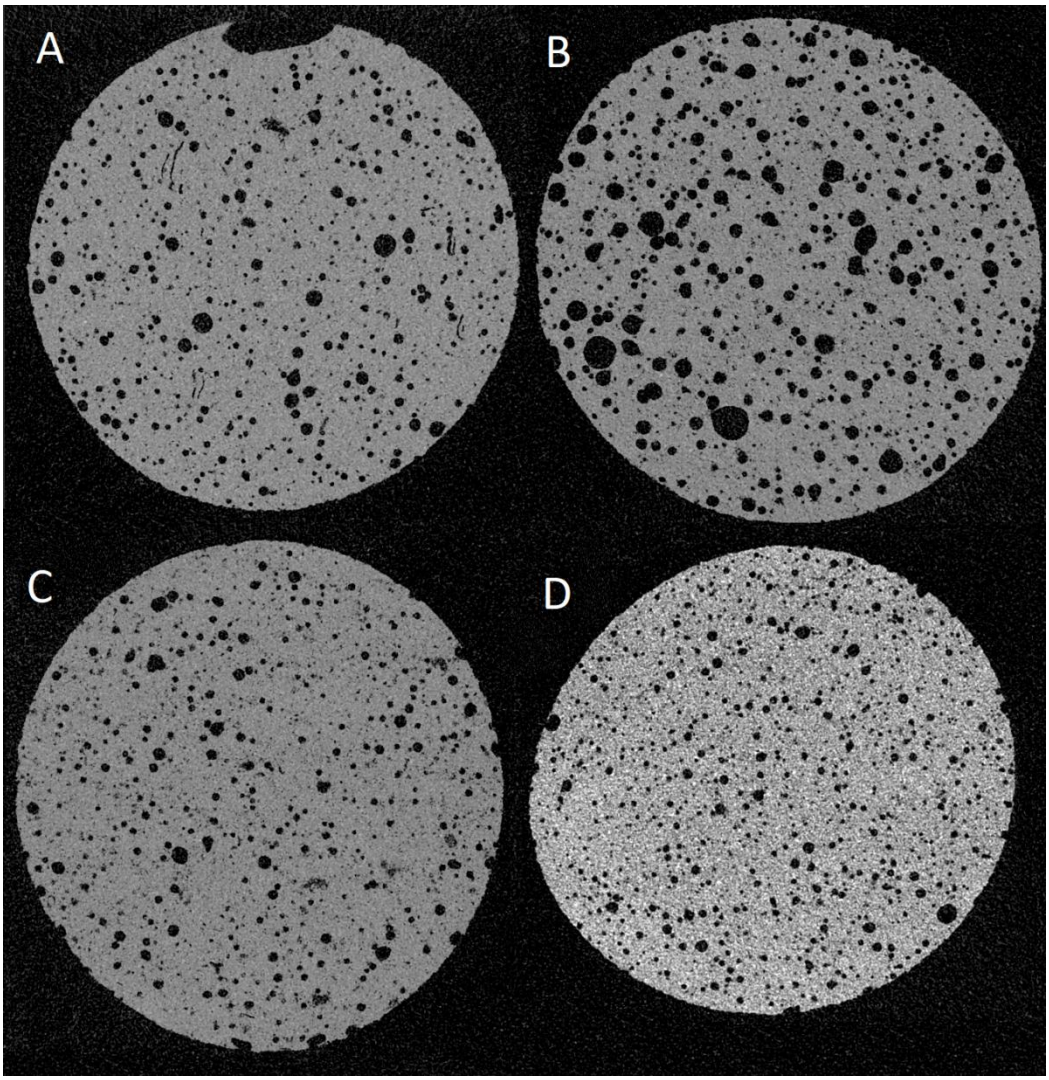

Figure 42: Micro-CT images of samples A: Dense control sample, B: Porous control sample, C: Dense 1 wt. % PCL-PLU fibers reinforced sample, D: Porous 1 wt. % PCL-PLU fibers reinforced sample.

5.6. FTIR analysis

Fourier transformed infra red spectroscopy is a complementary method, used to establish the presence and characteristic vibrations of functional groups. For the purpose of the thesis, this method was used for semi-quantitative determination of fiber content as well as presence of fibers.

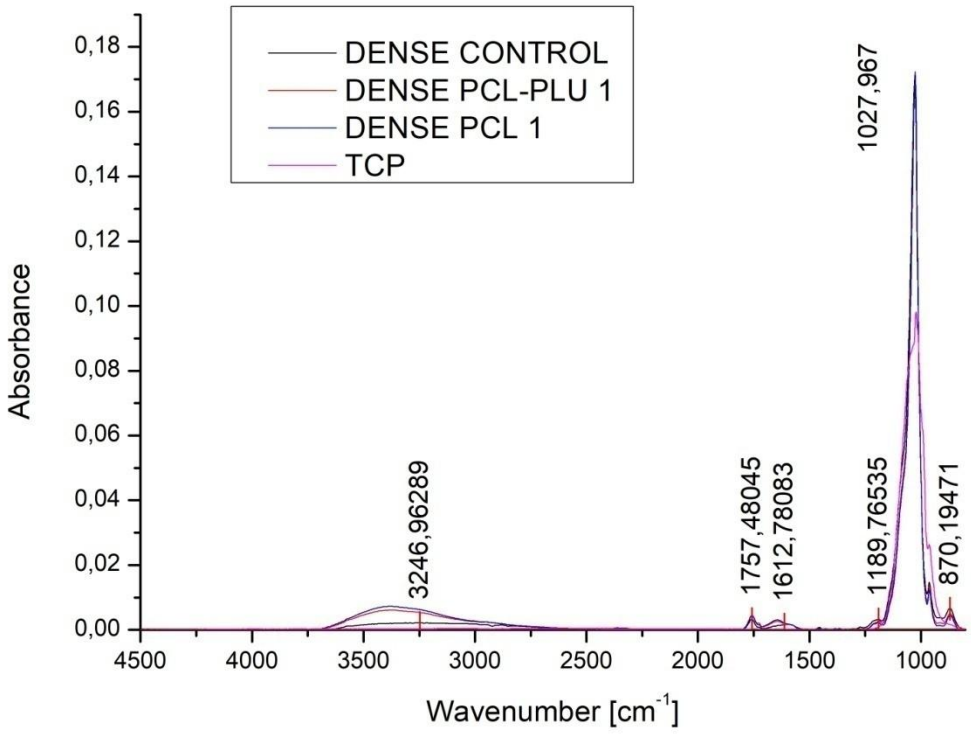

Figure 43: FTIR spectra of dense samples compared to α-TCP spectrum.

Comparison of pure α-TCP infrared spectrum to dense samples spectra showed different responses. Stretching at around 3500-3000 cm^{-1} was attributed to the presence of –OH groups present in CDHA and degradation products of thixotropic PLGA-PEG-PLGA. Peaks at 1757 and 1189 cm^{-1} were identified as the presence of carbonyl group probably originating from –CO-O- ester group and/or acidic –COOH group. This was to be expected, due to degradation of PLGA-PEG-PLGA copolymer to biodegradable polyethylene glycol, lactic and glycolic acids, or not yet degraded copolymer chain containing ester bonds. For fiber reinforced samples slightly higher peak stretching at 1612 cm^{-1} was observed. This stretching was attributed to carbonyl group from polymer fibers. A new peak at 870 cm^{-1} was identified as HPO_4 group stretching emerging in the spectrum from the reaction of α-TCP with water to CDHA respectively.

Porous samples with varying fiber contents showed similar spectra which more or less overlapped and contained all the observed and discussed peaks found in dense samples as well. Higher absorbance the values of control sample at –OH stretching might be explained by the use of more material for analysis. The significant peak at 1724 cm^{-1} as well as small peaks in the fingerprint region emerged with presence of fiber reinforcements in samples. These peaks were identified as PCL peaks enclosed in Figures 44 and 45 for comparison.

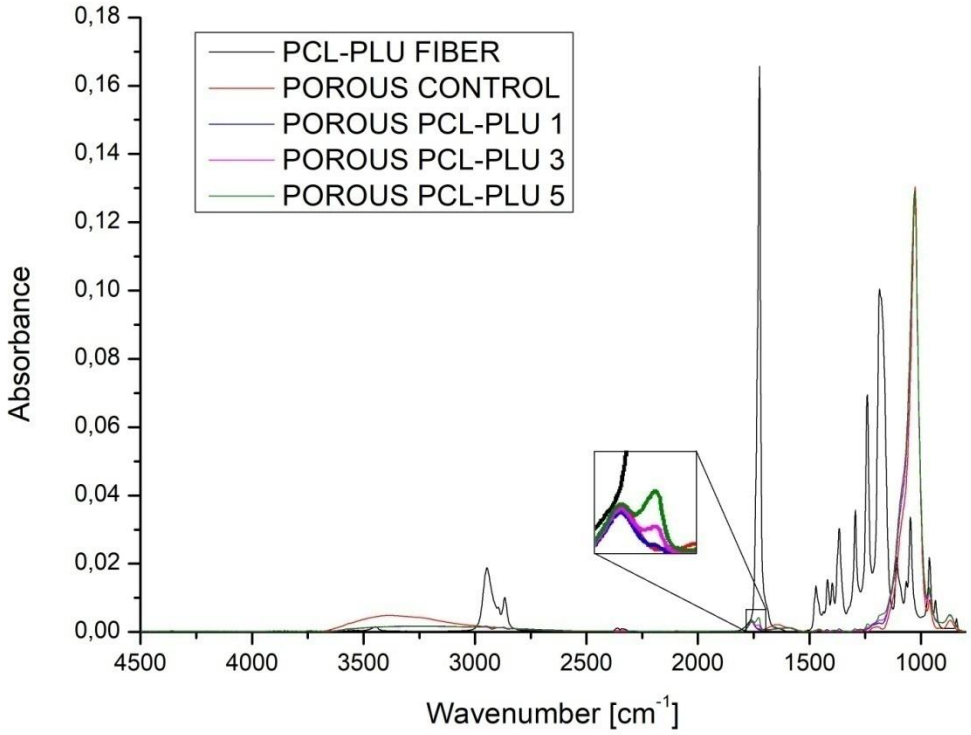

Figure 44: FTIR spectra of porous PCL-PLU reinforced samples with pure fiber spectrum for comparison.

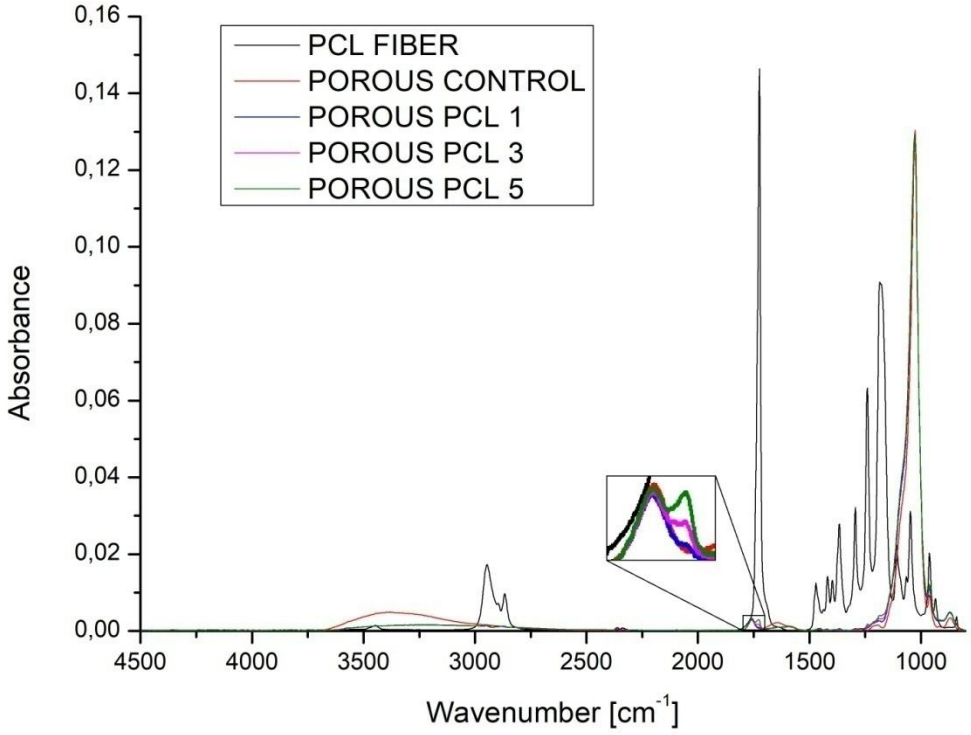

Figure 45: FTIR spectra of porous PCL reinforced samples with pure fiber spectrum for comparison.

As discussed earlier, FTIR can be used for semi-quantitative analysis. Analysis for this particular instance is based on the relation of 1724 cm^{-1} peak absorbance, corresponding to PCL fiber, which changes with fiber content. Plotting these values results in absorbance to fiber content relation displayed in Figure 46; this might be used for quantitative analysis as a calibration curve. Coefficients of determination (R^2) were established, nonetheless, for quantitative analysis values of R^2 are expected to be 0.999. Therefore, the presence of fibers was proved but fiber content is considered just semi-quantitative. Better homogeneity of fibers in the sample and use of the same quantity of sample for analysis can improve the sensitivity of the measurement.

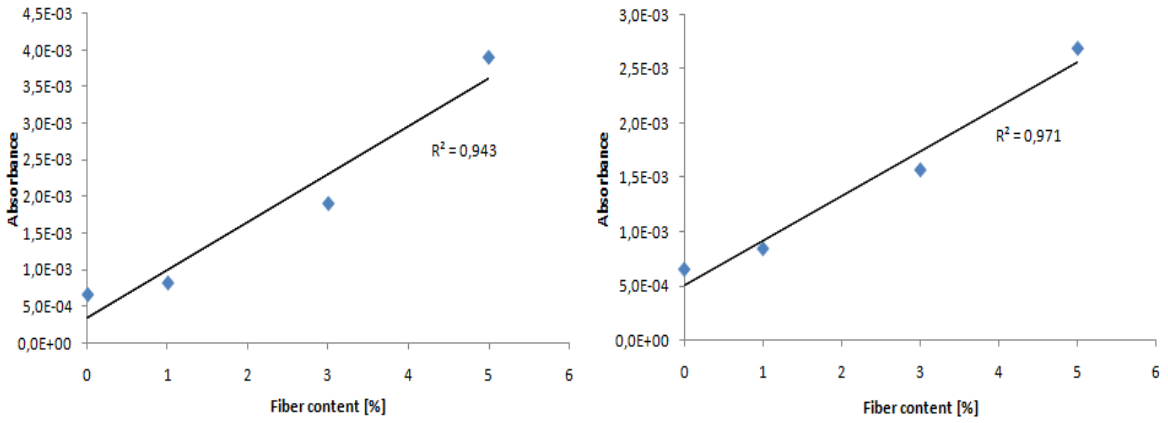

Figure 46: Semi-quantitative absorbance to fiber content relation of 1724 cm^{-1} peak for PCL-PLU reinforced samples (left) and PCL reinforced samples (right).

5.7. Setting kinetics and specification of crystalline composition

XRD analysis provided information about the transformation of α-TCP to CDHA, as well as phase crystalline composition of tested samples. Obtained data were evaluated on the basis of peak intensity using the external standard method according to an article by Ginebra et al. [58].

Phase change from α-TCP to CDHA was studied and setting kinetics established. As seen in Figure 47, with increasing reaction time, intensities for characteristic peaks of unreacted α-TCP at 12.10, 14.02, 15.16, 22.20, 24.10, and 30.74 ° 2θ decrease and apatite peaks appear with increasing intensity. This proves the transformation, and it is possible to establish α-TCP to CDHA conversion according to equations 10 and 11 below, where w_t is weight fraction of α-TCP in time t, I_t is peak intensity in time t, I_0 is peak intensity of unreacted α-TCP, M_{CDHA} and $M_{\alpha\text{-TCP}}$ is mass attenuation coefficient in cm^2/g.

$$w_t = \frac{I_t M_{CDHA}}{M_{\alpha-TCP}\, I_0 - I_t (M_{\alpha-TCP} - M_{CDHA})} \tag{10}$$

$$R_t = \frac{w_0 - w_t}{w_0} \cdot 100 \tag{11}$$

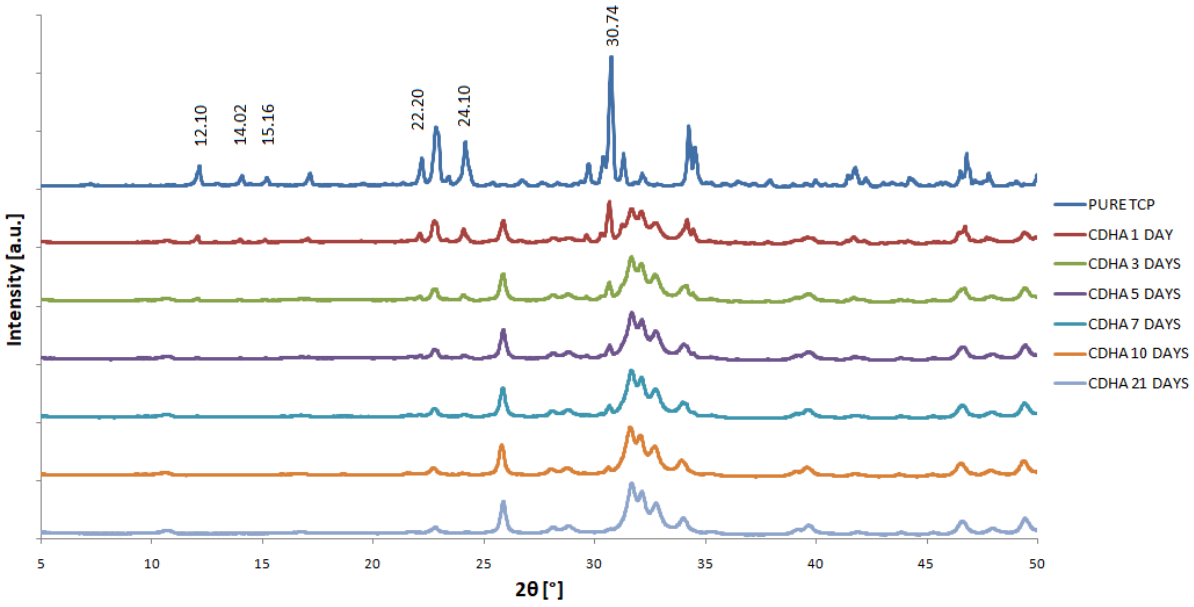

Figure 47: Diffraction patterns of samples with different setting times and pure α-TCP as a reference,

Intensity variations of the most dominant peak at 30.74 ° 2θ were used to produce R_t. Plotting R_t against setting time produced so-called the extent of conversion. After 1 day, conversion reached 78 %, indicating rapid dissolution and transformation of fine α-TCP particles. Rate of conversion gradually decreased in time. After 10 days of setting at physiological conditions in the incubator, conversion reached 92 %. 10 days of setting time was therefore, considered as optimal setting time and used in experiments.

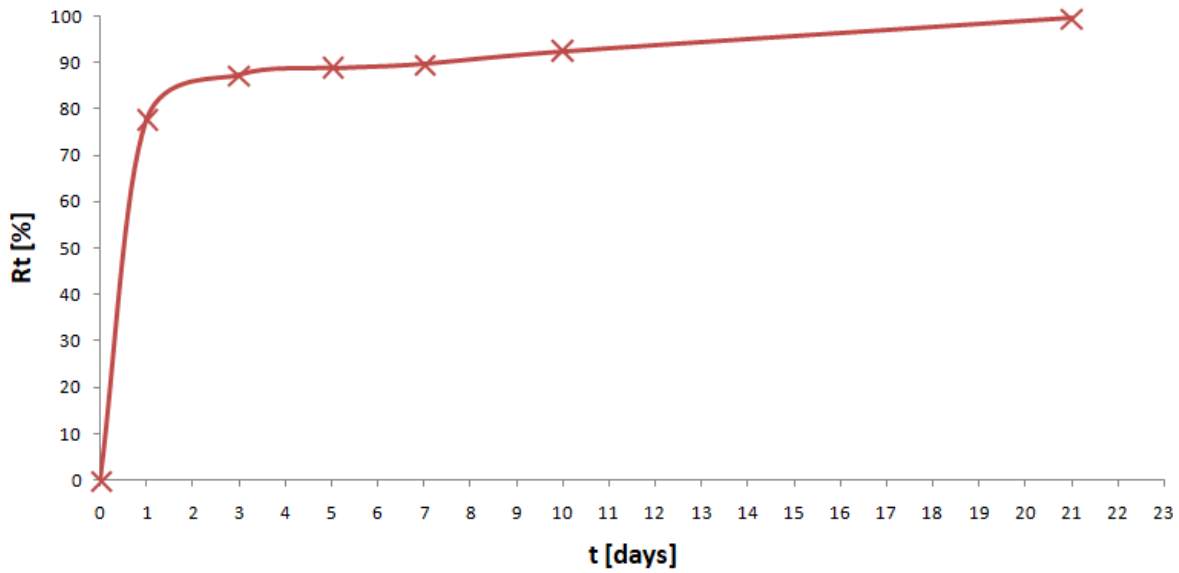

Figure 48: Extent of conversion as a function of setting time.

As seen in Figures 49, 50 and 51, diffraction curves of prepared samples do indeed overlap. Transformation, therefore, came through, and polymer fibers did not interfere with the setting of cement paste, at least not in mineralogical sense. For reference, diffractogram of α-TCP is also included in Figures. It is possible to observe, that characteristic peaks for α-TCP are missing or are greatly repressed in case of peaks at 22.20 and 30.74 2θ °. This indicates the total or almost total transformation of α-TCP to CDHA.

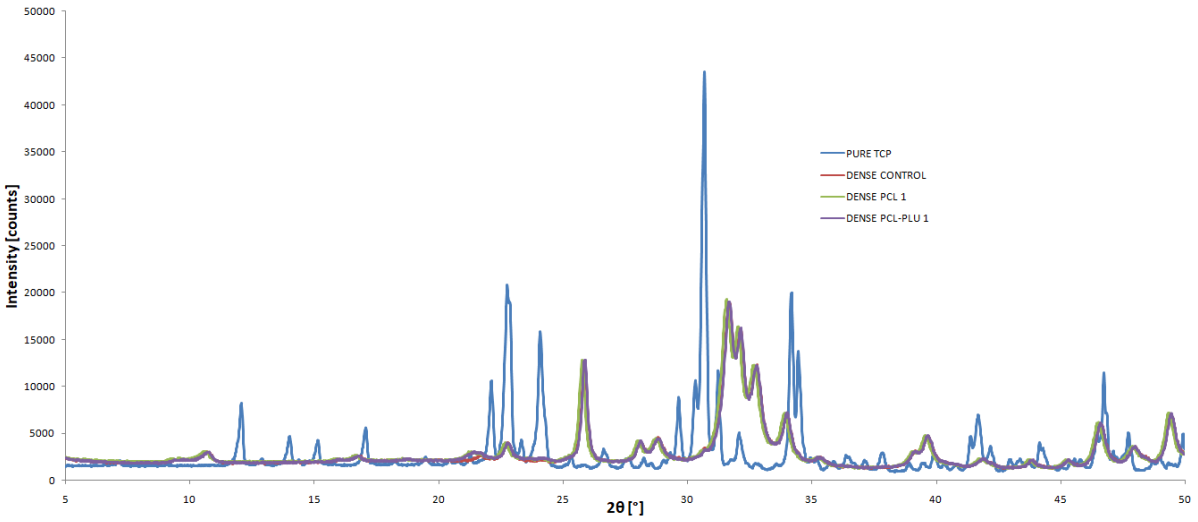

Figure 49: XRD diffractograms of dense samples with α-TCP diffractogram for reference.

In reinforced samples, the emergence of peaks at 21.36 and 23.66 2θ ° has been observed. Because PCL and PCL-PLU modified fibers are semi-crystalline polymers, they scatter the X-rays which show in diffractograms. These peaks were therefore, identified as reinforcing fibers. Interestingly, intensities of these two peaks are directly correlated to fiber content. Due to PCL fiber's slightly more semi-crystalline nature than its modified counterpart, intensities of two corresponding fiber contents are higher for PCL reinforced samples. This fact is most observable for porous samples with varying fiber content. Nonetheless, detected fiber inhomogeneity from individual sample to another sample can also explain this observed phenomenon.

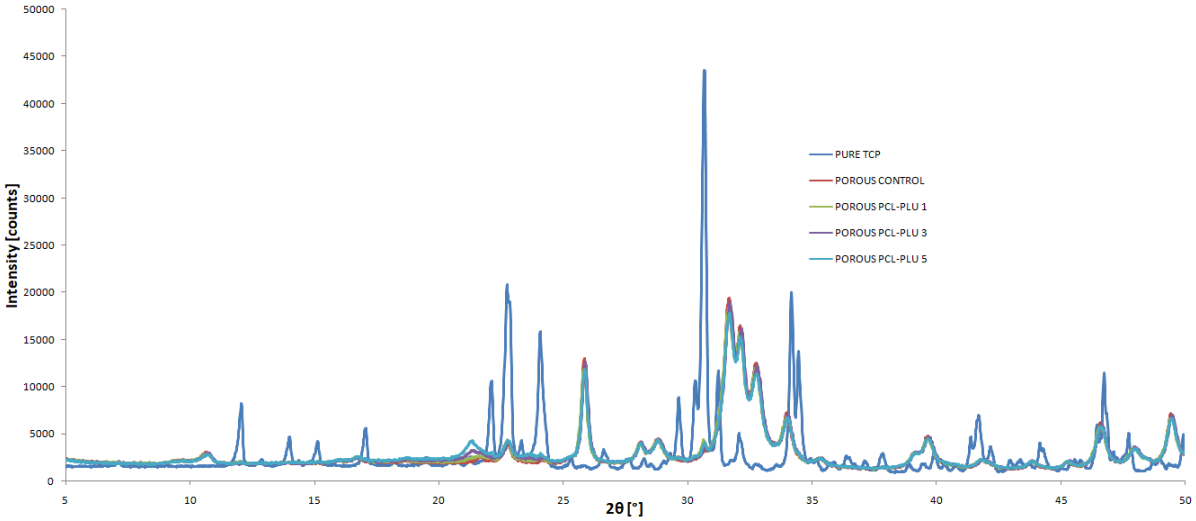

Figure 50: XRD diffractograms of porous samples reinforced with PCL-PLU fibers.

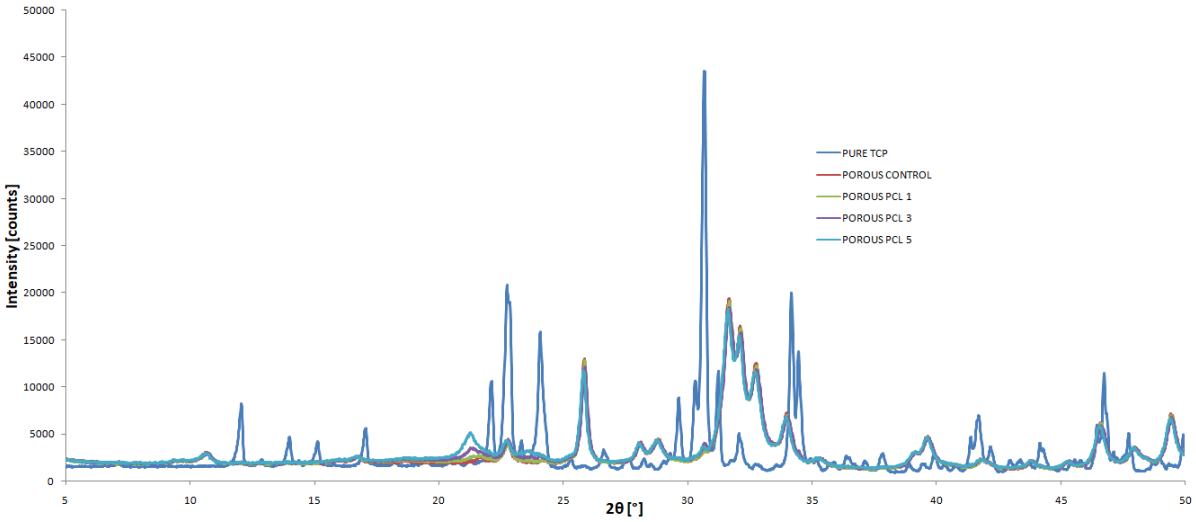

Figure 51: XRD diffractograms of porous samples reinforced with PCL fibers.

6. CONCLUSION

The aim of the work was to evaluate mechanical and rheological aspects of biodegradable fiber reinforced phosphate cement. It has been found that polymer fibers do indeed interfere with paste rheological properties, increase in initial storage modulus with higher fiber content was confirmed, but fibers did not interfere final product of setting. Whenever fiber content exceeded 3 wt. %, paste proved to be too difficult to inject via syringe, while losing its potential application in surgical practice.

Two types of sample mixing techniques were tested – spatula mixing and speed-stirring mixing. Porosity and pore distribution did in fact increase for speed-stirred "porous" samples, compared to spatula mixed "dense". This finds applications in osteoconductivity domain, where cells are prone to adhere better to the porous material. However decrease in porosity with addition of fiber reinforcements was observed. Homogeneity of fibers inside the ceramic matrix also increased in porous samples.

Performance of PCL and PCL-Pluronic modified fibers was tested as well, and PCL-Pluronic modified fibers showed slightly better performance at lower additions compared to PCL fibers, possibly due to their amphiphilic nature.

Mechanical properties of reinforced cement samples showed a slight increase in compressive strength domain, namely for samples reinforced with 3 wt. % PCL-Pluronic modified polymer fibers. Diametrical tensile strength tests were conducted, but obtained results and consecutive SEM images of crack surfaces proved that all the fiber reinforcement capabilities were quite low. Samples performed better in the dry state compared to the wet state; the wet ceramic matrix was more brittle and fibers did not have a significant effect on mechanical parameters under physiological conditions. Due to higher porosity of porous samples, observed clumping of fibers, and possible fiber inhomogeneity originating from sample preparation were mechanical properties greatly impaired.

Setting kinetics was established and the transformation of α-TCP to CDHA was proved. After 10 days of setting under physiological conditions 92 % of α-TCP already transformed to CDHA. The statement was supported by XRD diffractograms and images from SEM. This setting time was reproduced for every sample with varying fiber content. Due to fiber semi-crystalline nature, peaks at 21.36 and 23.66 ° 2θ were observed and their intensities were correlated to fiber content. FTIR analysis also proved fiber presence in sample structure. Absorbance for characteristic peaks of PCL at 1724 cm^{-1} was directly correlated to fiber content, serving the purpose of semi-quantitative analysis.

In conclusion, the increased fiber content did in fact decrease paste injectability and only a slight increase in mechanical parameters was observed. A most promising candidate for surgical practice seems to be 3 wt. % PCL-Pluronic modified fiber additive where significant statistical increase in compressive strength was recorded. However, poor matrix-fiber adhesion was recorded as well. Different fiber type, fiber morphology or size and fiber homogeneity in the ceramic matrix might provide better reinforcing capabilities than tested PCL and PCL-Pluronic fibers. However, for temporary fixation of bone defect, injectable and biodegradable calcium phosphate cement paste still seems to be a better alternative than PMMA counterpart, at least from the biological and long term stand point.

Lastly, further research into the topic is required, especially to mechanical parameters, porosity, in vivo behavior and injectability, to fine-tune properties and performance of this material.

7. REFERENCES

[1] STEELE, D. Gentry a Claud A BRAMBLETT. *The anatomy and biology of the human skeleton*. College Station: Texas A&M University Press, c1988. ISBN 0-89096-300-2.

[2] ČECH, Svatopluk a Drahomír HORKÝ. *A obecné histologie*. 2., přeprac. vyd. Brno: Masarykova univerzita, 2011. ISBN 978-80-210-5543-8.

[3] Childhood Acute Myeloid Leukemia Treatment (PDQ®)—Patient Version - National Cancer Institute. Comprehensive Cancer Information - National Cancer Institute [online]. From: https://www.cancer.gov/types/leukemia/patient/child-aml-treatment-pdq?utm_content=sf27145602&utm_medium=spredfast&utm_source=facebook&utm_campaign=National%20Cancer%20Institute&cid=sf27145602&redirect=true

[4] YOUNG, Barbara. Wheater's functional histology: a text and colour atlas. 5th ed. Edinburgh?: Churchill Livingstone/Elsevier, 2006. ISBN 978-0-443-068-508.

[5] Cooper, D.M.L., Kawalilak, C.E., Harrison, K. et al. Curr Osteoporos Rep (2016) 14: 187. https://doi.org/10.1007/s11914-016-0319-y

[6] Types of Bone Fractures: Buckle Fracture, Stress Fracture, Comminuted Fracture, and More. WebMD - Better information. Better health. [online]. Copyright © 2005 [cit. 03.11.2018]. From: https://www.webmd.com/a-to-z-guides/understanding-fractures-basic-information

[7] TOWNSEND, Courtney, R. Daniel BEAUCHAMP, B. Mark EVERS a Kenneth MATTOX. Sabiston Textbook of Surgery: The Biological Basis of Modern Surgical Practice. 20th Edition. Philladelphia: Elsevier, 2016. ISBN 978-0-323-40162-3.

[8] IVERGÅRD, M., J. COMPSTON a C. COOPER. Osteoporosis in the European Union: medical management, epidemiology and economic burden: A report prepared in collaboration with the International Osteoporosis Foundation (IOF) and the European Federation of Pharmaceutical Industry Associations (EFPIA). Archives of Osteoporosis. 2013, 2013(8:136). DOI: DOI 10.1007/s11657-013-0136-1.

[9] Osteoporosis. Www.niams.nih.gov [online]. National Institutes of Health, 9000 Rockville Pike, Bethesda, Maryland 20892, 2016 [cit. 2018-11-03]. From: https://www.niams.nih.gov/health-topics/osteoporosis#tab-causes

[10] SHIRTLIFF, Mark. Osteomyelitis of the Long Bones. Seminars in Plastic Surgery. 2009, 2009(23(2):59-7). DOI: DOI: 10.1055/s-0029-1214158.

[11] Total Hip Replacement – USC Viterbi School of Engineering. USC Viterbi School of Engineering – USC Viterbi School of Engineering [online]. From: https://illumin.usc.edu/total-hip-replacement/

[12] FREEMAN, M. A. R., G. W. BRADLEY a P. A. REVELL. OBSERVATIONS UPON THE INTERFACE BETWEEN BONE AND POLYMETHYLMETHACRYLATE CEMENT. THE JOURNAL OF BONE AND JOINT SURGERY. 1982, 1982(Vol. 64-B), 489-493.

[13] KAUFMANN, Timothy J., Mary E. JENSEN, Gabriele FORD, Lena L. GILL, William F. MARX a David F. KALLAMES. Cardiovascular Effects of Polymethylmethacrylate Use in Percutaneous Vertebroplasty. American Journal of Neuroradiology. 2002, 23(4), 601-604.

[14] HK XU, Hockin, Ping WANG, Lin WANG, et al. Calcium phosphate cements for bone engineering and their biological properties. Bone Research. 2017, 2017(5). DOI: doi:10.1038/boneres.2017.56.

[15] ZHANG, Jingtao, Weizhen LIU, Verena SCHNITZLER, Franck TANCRET a Jean MICHELBOULER. Calcium phosphate cements for bone substitution: Chemistry,

handling and mechanical properties. Acta Biomaterialia. 2014, 2014(Volume 10, 3), 1035-1049. DOI: https://doi.org/10.1016/j.actbio.2013.11.001. ISSN 1742-7061.
[16] UNUMA, Hidero a Yuta MATSUSHIMA. Preparation of calcium phosphate cement with an improved setting behavior. Journal of Asian Ceramic Societies. 2018, 2013(1), 26-29. DOI: https://doi.org/10.1016/j.jascer.2013.02.003.
[17] BLOKHUIS, T.J. Bioresorbable bone graft substitutes. Bone Substitute Biomaterials [online]. Elsevier, 2014, 2014, s. 80-92 [cit. 2019-01-04]. DOI: 10.1533/9780857099037.1.80. ISBN 9780857094971. From: https://linkinghub.elsevier.com/retrieve/pii/B9780857094971500044
[18] CARRODEGUAS, R.G. a S. DE AZA. A-Tricalcium phosphate: Synthesis, properties and biomedical applications. *Acta Biomateralia*[online]. 2011, **7**(10), 3536–3546 [cit. 2019-01-08]. DOI: https://doi.org/10.1016/j.actbio.2011.06.019. From: https://www.sciencedirect.com/science/article/pii/S174270611100256X
[19] MATHEW, M. The crystal structure of [alpha]-Ca3(PO4)2. *Acta Crystallographica* [online]. 1977, **33**, 1325-1333 [cit. 2019-01-14]. DOI: https://doi.org/10.1107/S0567740877006037. From: http://scripts.iucr.org/cgi-bin/paper?S0567740877006037
[20] YASHIMA, Masamoto. Crystal structure analysis of β-tricalcium phosphate Ca3(PO4)2 by neutron powder diffraction. *Journal of Solid State Chemistry* [online]. 2003, **175**(2), 272-277 [cit. 2019-01-08]. DOI: https://doi.org/10.1016/S0022-4596(03)00279-2. From: https://www.sciencedirect.com/science/article/pii/S0022459603002792
[21] YASHIMA, Masamoto. High-temperature neutron powder diffraction study of the structural phase transition between α and α′ phases in tricalcium phosphate Ca3(PO4)2. *Chemical Physics Letters* [online]. 2003, **372**(5-6), 779-783 [cit. 2019-01-08]. DOI: https://doi.org/10.1016/S0009-2614(03)00505-0. From: https://www.sciencedirect.com/science/article/pii/S0009261403005050 [22]
[22] SU, Wen-Yu a Feng-Huei LIN. A New Type of Biphasic Calcium Phosphate Cement as a Gentamicin Carrier for Osteomyelitis. Evidence-Based Complementary and Alternative Medicine [online]. 2013, 2013 [cit. 2019-01-09]. DOI: http://dx.doi.org/10.1155/2013/801374. From: https://www.researchgate.net/publication/236676232_A_New_Type_of_Biphasic_Calcium_Phosphate_Cement_as_a_Gentamicin_Carrier_for_Osteomyelitis
[23] BHATNAGAR, V. M. Infrared spectrum of strontium hydroxyapatite. *Experientia* [online]. 1967, **23**(9), 697-699 [cit. 2019-01-09].
[24] JOKIC, B. Synthesis and settings behavior of α-TCP from calcium deficient hyroxyapatite obtained by hydrothermal method. JOURNAL OF OPTOELECTRONICS AND ADVANCED MATERIALS [online]. 2007, 9(6), 1904-1910 [cit. 2019-01-10]. From: http://joam.inoe.ro/download.php?idu=371
[25] AYERS, Reed. Osteoblast-like cell mineralization induced by multiphasic calcium phosphate ceramic. *Materials Science and Engineering: C* [online]. 2006, **26**(8), 1333-1337 [cit. 2019-01-10]. DOI: https://doi.org/10.1016/j.msec.2005.08.028. From: https://www.sciencedirect.com/science/article/pii/S0928493105002055
[26] VOLKMER, T.M. Obtainment of α-tricalcium phosphate by solution combustion synthesis method using urea as combustible. *Key Engineering Materials*[online]. 2008, **396-398**, 591-594 [cit. 2019-01-10]. DOI: DOI: 10.4028/www.scientific.net/KEM.396-398.591. From: https://www.researchgate.net/publication/250328093_Obtainment_of_a-Tricalcium_Phosphate_by_Solution_Combustion_Synthesis_Method_Using_Urea_as_Combustible

[27] CARRODEGUAS, Raúl García. New Approach to the β→α Polymorphic Transformation in Magnesium-Substituted Tricalcium Phosphate and its Practical Implications. *Journal of American Ceramic Society* [online]. 2008, **91**(4), 1281-1286 [cit. 2019-01-14]. DOI: https://doi.org/10.1111/j.1551-2916.2008.02294.x. From: https://ceramics.onlinelibrary.wiley.com/doi/full/10.1111/j.1551-2916.2008.02294.x

[28] MOTISUKE, M. Mg-free precursors for the synthesis of pure phase Si-doped a-Ca 3(PO4)2. *Key Engineering Materials* [online]. 2008, **361-363**, 199-202 [cit. 2019-01-14]. DOI: 10.4028/www.scientific.net/KEM.361-363.199. From: https://www.researchgate.net/publication/233392108_Mg-Free_Precursors_for_the_Synthesis_of_Pure_Phase_Si-Doped_a-Ca3PO42sub

[29] NURSE, R. W. High-temperature phase equilibria in the system dicalcium silicate–tricalcium phosphate. *Journal of Chemical Society*[online]. 1959, **220** [cit. 2019-01-14]. DOI: 10.1039/JR9590001077. From: https://www.researchgate.net/publication/250857685_High-Temperature_Phase_Equilibria_in_the_System_Dicalcium_Silicate-Tricalcium_Phosphate

[30] WANG, Lijun a George H. NANCOLLAS. Calcium Orthophosphates: Crystallization and Dissolution. *Chemical Reviews* [online]. 2008, **108**(11), 4628-4669 [cit. 2019-01-19]. DOI: 10.1021/cr0782574. ISSN 0009-2665. From: http://pubs.acs.org/doi/abs/10.1021/cr0782574

[31] CASTRO, Antonio G.B. Incorporation of PLLA micro-fillers for mechanical reinforcement of calcium-phosphate cement. *Journal of the Mechanical Behavior of Biomedical Materials* [online]. 2017, **71**, 286-294 [cit. 2019-01-21]. DOI: http://dx.doi.org/10.1016/j.jmbbm.2017.03.027. From: https://reader.elsevier.com/reader/sd/pii/S1751616117301479?token=1212F23AB0BEF4EB61AA36C455F64F72BC1B25B66A8062C334E29EF58D23769F7606B6E8B0CC8105D2D6531F4A3A1E00

[32] PANZAVOLTA, S. a Maria Letizia FOCARETE. Fiber reinforcement of a biomimetic bone cement. *Journal of Materials Science Materials in Medicine* [online]. 2012, **23**(6), 1363–1370 [cit. 2019-01-23]. DOI: DOI: 10.1007/s10856-012-4618-2. From: https://www.researchgate.net/publication/224820938_Fiber_reinforcement_of_a_biomimetic_bone_cement

[33] YANG, Boyuan. Effect of ultrafine poly(ε-caprolactone) fibers on calcium phosphate cement: in vitro degradation and in vivo regeneration. International Journal of Nanomedicine [online]. 2016, 2016(11), 163-177 [cit. 2019-01-23]. DOI: https://doi.org/10.2147/IJN.S91596. From: https://www.dovepress.com/effect-of-ultrafine-polyepsilon-caprolactone-fibers-on-calcium-phospha-peer-reviewed-article-IJN

[34] CANAL, C. a M.P. GINEBRA. Fibre-reinforced calcium phosphate cements: A review. *Journal of the Mechanical Behavior of Biomedical Materials* [online]. 2011, **4**(8), 1658-1671 [cit. 2019-01-23]. DOI: https://doi.org/10.1016/j.jmbbm.2011.06.023. From: https://www.sciencedirect.com/science/article/pii/S1751616111001810

[35] Sigma-Aldrich: Analytical, Biology, Chemistry & Materials Science products and services. | Sigma-Aldrich [online]. From: https://www.sigmaaldrich.com/catalog/product/aldrich/805211?lang=en®ion=CZ

[36] MARK, James E. *Physical properties of polymers handbook*. 2nd ed. New York: Springer, 2006. ISBN 0387312358.

[37] HANNINK, Gerjon a J.J. Chris ARTS. Bioresorbability, porosity and mechanical strength of bone substitutes: What is optimal for bone regeneration?. *Injury* [online]. 2011, **42**(Supplement 2), S22-S25 [cit. 2019-01-28]. DOI: https://doi.org/10.1016/j.injury.2011.06.008. From: https://www.sciencedirect.com/science/article/pii/S0020138311002452

[38] VOJTOVA, L. The Effect of the Thermosensitive Biodegradable PLGA–PEG–PLGA Copolymer on the Rheological, Structural and Mechanical Properties of Thixotropic Self-Hardening Tricalcium Phosphate Cement. *International Journal of Molecular Sciences*[online]. 2019, **20**(2), 391 [cit. 2019-01-28]. DOI: doi:10.3390/ijms20020391. From: https://www.mdpi.com/1422-0067/20/2/391

[39] CHAMRADOVA, I. The effect of hydroxyapatite particle size on viscoelastic properties and calcium release from a thermosensitive triblock copolymer. *Colloid and Polymer Science* [online]. 2016, **295**(1), 107-115 [cit. 2019-01-28]. DOI: DOI 10.1007/s00396-016-3983-7. From: https://link.springer.com/content/pdf/10.1007%2Fs00396-016-3983-7.pdf

[40] MICHLOVSKÁ, L. Functionalization Conditions of PLGA-PEG-PLGA Copolymer with Itaconic Anhydride. *New Frontiers in Macromolecular Science: Special Issue* [online]. 2010, **295**(1), 119-124 [cit. 2019-01-31]. DOI: https://doi.org/10.1002/masy.200900071. From: https://onlinelibrary.wiley.com/doi/full/10.1002/masy.200900071

[41] DEL REAL, R.P. A new method to produce macropores in calcium phosphate cements. *Biomaterials* [online]. 2002, **23**(17), 3673-3680 [cit. 2019-01-31]. DOI: https://doi.org/10.1016/S0142-9612(02)00101-1. From: https://www.sciencedirect.com/science/article/pii/S0142961202001011

[42] BOSE, Susmita a Solaiman TARAFDER. Calcium phosphate ceramic systems in growth factor and drug delivery for bone tissue engineering: A review. *Acta Biomaterialia* [online]. 2011, **8**(4), 1401–1421 [cit. 2019-02-02]. DOI: 10.1016/j.actbio.2011.11.017. From: https://www.sciencedirect.com/science/article/pii/S1742706111005046?via%3Dihub#f0005

[43] PELLETIER, Matthew H. The Compressive Properties of Bone Cements Containing Large Doses of Antibiotics. The Journal of Arthroplasty [online]. 2009, 24(3), 454-460 [cit. 2019-02-02]. DOI: https://doi.org/10.1016/j.arth.2007.10.023. From: https://www.sciencedirect.com/science/article/pii/S0883540307006286?via%3Dihub

[44] XU, Hison. Reinforcement of a Self Setting Calcium Phosphate Cement With Different Fibers. *Journal of Biomedical Materials Research*[online]. 2000, **52**(1), 107-14 [cit. 2019-02-05]. DOI: 10.1002/1097-4636(200010)52:13.3.CO;2-S. From: https://www.researchgate.net/publication/12412126_Reinforcement_of_a_Self_Setting_Calcium_Phosphate_Cement_With_Different_Fibers

[45] WANG, Xiupeng a Jiandong YE. Reinforcement of calcium phosphate cement by bio-mineralized carbon nanotube. *Journal of American Ceramic Society* [online]. 2007, **90**(3), 962-964 [cit. 2019-02-05]. DOI: https://doi.org/10.1111/j.1551-2916.2006.01460.x. From: https://ceramics.onlinelibrary.wiley.com/doi/full/10.1111/j.1551-2916.2006.01460.x

[46] CHEW, Kean-Khoon. Reinforcement of calcium phosphate cement with multi-walled carbon nanotubes and bovine serum albumin for injectable bone substitute applications. *Journal of the Mechanical Behavior of Biomedical Materials* [online]. 2011, **4**(3), 331-339 [cit. 2019-02-05]. DOI: https://doi.org/10.1016/j.jmbbm.2010.10.013. From: https://www.sciencedirect.com/science/article/pii/S175161611000161X?via%3Dihub

[47] Schematic representation of single walled carbon nanotube (SWCNT) and... | Download Scientific Diagram. ResearchGate | Share and discover research [online]. Copyright © ResearchGate [cit. 05.02.2019]. From: https://www.researchgate.net/figure/Schematic-representation-of-single-walled-carbon-nanotube-SWCNT-and-multi-walled-carbon_fig1_319966218
[48] MIRHOSSEINI, M. M. Fabrication and characterization of hydrophilic poly(ε-caprolactone)/pluronic P123 electrospun fibers. Journal of Applied Polymer Science [online]. 2016, 133(7) [cit. 2019-02-07]. DOI: https://doi.org/10.1002/app.43345. From: https://onlinelibrary.wiley.com/doi/10.1002/app.43345
[49] MAAZOUZA, Yassine a Edgar B. MONTUFAR. Self-hardening and thermoresponsive alpha tricalcium phosphate/pluronic pastes. Acta Biomaterialia [online]. 2017, 49(2017), 563-574 [cit. 2019-02-07]. DOI: https://doi.org/10.1016/j.actbio.2016.11.043. From: https://www.sciencedirect.com/science/article/pii/S1742706116306407?via%3Dihub
[50] PITTO-BARRY, Anaïs a Nicolas P. E. BARRY. Pluronic® block-copolymers in medicine: from chemical and biological versatility to rationalisation and clinical advances. Polymer Chemistry [online]. 2014, 5(10), 3291-3297 [cit. 2019-02-07]. DOI: 10.1039/C4PY00039K. From: https://pubs.rsc.org/en/content/articlepdf/2014/py/c4py00039k
[51] LYNGE, Martin E a Rebecca van der WESTEN. Polydopamine—a nature-inspired polymer coating for biomedical science. Nanoscale[online]. 2011, 3(12), 4916-4928 [cit. 2019-02-10]. DOI: DOI: 10.1039/c1nr10969c. From: https://pubs.rsc.org/en/content/articlepdf/2011/nr/c1nr10969c
[52] DOROZHKIN, Sergey V. Calcium orthophosphate cements for biomedical application. *Journal of Materials Science* [online]. 2008, **43**(9), 3028-3057 [cit. 2019-02-11]. DOI: 10.1007/s10853-008-2527-z. From: https://link.springer.com/article/10.1007/s10853-008-2527-z
[53] AMBAR, Alberto J. Calcium Phosphate Cement: Review ofMechanical and Biological Properties. Journal of Prosthodontics [online]. 2006, 15(5), 321-328 [cit. 2019-02-11]. DOI: 10.1111/j.1532-849X.2006.00129.x. From: https://onlinelibrary.wiley.com/doi/epdf/10.1111/j.1532-849X.2006.00129.x
[54] ZHANG, Weibo. The formation of tertiary dentin after pulp capping with a calcium phosphate cement, loaded with PLGA microparticles containing TGF-β1. Journal of Biomedical Materials Research [online]. 2008, 85A(2), 439-444 [cit. 2019-02-11]. DOI: https://doi.org/10.1002/jbm.a.31558. From: https://onlinelibrary.wiley.com/doi/full/10.1002/jbm.a.31558
[55] GINEBRA, Maria-Pau. Calcium phosphate cements as drug delivery materials. Advanced Drug Delivery Reviews [online]. 2012, 64(12), 1090-1100 [cit. 2019-03-06]. DOI: https://doi.org/10.1016/j.addr.2012.01.008. From: https://www.sciencedirect.com/science/article/pii/S0169409X12000117?via%3Dihub
[56] The Polymer Science Learning Center [online]. From: https://pslc.ws/macrog/pmma.htm
[57] Kyphoplasty | Rehab My Patient. Exercise prescription software for therapist | Rehab My Patient [online]. Copyright © 2019 RehabMyPatient.com [cit. 18.03.2019]. From: https://www.rehabmypatient.com/lumbar-spine/kyphoplasty
[58] GINEBRA, Marie-Pau. Setting Reaction and Hardening of an Apatitic Calcium Phosphate Cement. *Journal of Dental Research* [online]. 1997, **76**(5), 905-912 [cit. 2019-04-06]. DOI: https://doi.org/10.1177/00220345970760041201. From:

https://www.researchgate.net/publication/14092519_Setting_Reaction_and_Hardening_of_an_Apatitic_CPC
[59] SHOJA, M. PREPARATION AND CHARACTERIZATION OF POLY (εCAPROLACTONE)/TiO2 MICRO-COMPOSITES. Digest Journal of Nanomaterials and Biostructures [online]. 2015, 10(2), 471-477 [cit. 2019-04-16]. From: http://www.chalcogen.ro/471_Shoja.pdf
[60] LI, Wenchao a Yiqiang HU. Electrospinning of Polycaprolactone/Pluronic F127 dissolved in glacial acetic acid: fibrous scaffolds fabrication, characterization and in vitro evaluation. Journal of Biomaterials Science Polymer Edition [online]. 2018, 29(10), 1-24 [cit. 2019-05-06]. DOI: DOI: 10.1080/09205063.2018.1439431. From: https://www.researchgate.net/publication/323266583

8. ABBREVIATIONS

PMMA – poly(methyl methacrylate)
MMA – methyl methacrylate
CPC – calcium phosphate cement
DCPD – dicalcium phosphate dihydrate (brushite)
HA – hydroxyapatite
CDHA – calcium deficient hydroxyapatite
TCP – tricalcium phosphate
XRD – X-ray diffraction analysis
FTIR – Fourier transformed infrared spectroscopy
XANES – X-ray absorption near edge surface spectroscopy
MAS-NMR – magnetic angle spinning nuclear magnetic resonance
ACP – amorphous calcium phosphate
DCPA – anhydrous dicalcium phosphate (moneite)
OCP – octacalcium phosphate
TTCP – tetracalcium phosphate
CNT – carbon nanotubes
PLLA – poly(*levus*-lactic acid)
PLGA – poly(lactic-co-glycolic acid)
PCL – poly(ε-caprolactone)
PCL-PLU – poly(ε-caprolactone) modified with Pluronic
ROP – ring-opening polymerization
PDA – polydopamine
MIR-ATR – mid-infrared attenuated total reflectance
SEM – scanning electron microscopy
micro-CT – micro-computed tomography
SE – secondary electrons
BSE – backscattered electrons
PDI – polyidispersity index
M_n – number-average polymer molecular weight
M_w – mass-average polymer molecular weight
G’ – storage dynamic modulus
G’’ – loss dynamic modulus
q – individual fraction distribution
CS – compressive strength
E – Young’s elastic modulus
DTS – diametrical tensile strength

9. THE LIST OF FIGURES

10. THE LIST OF TABLES